Article

Structure

Cryo-EM Structure of the Prostaglandin E Receptor EP4 Coupled to G Protein

Graphical Abstract

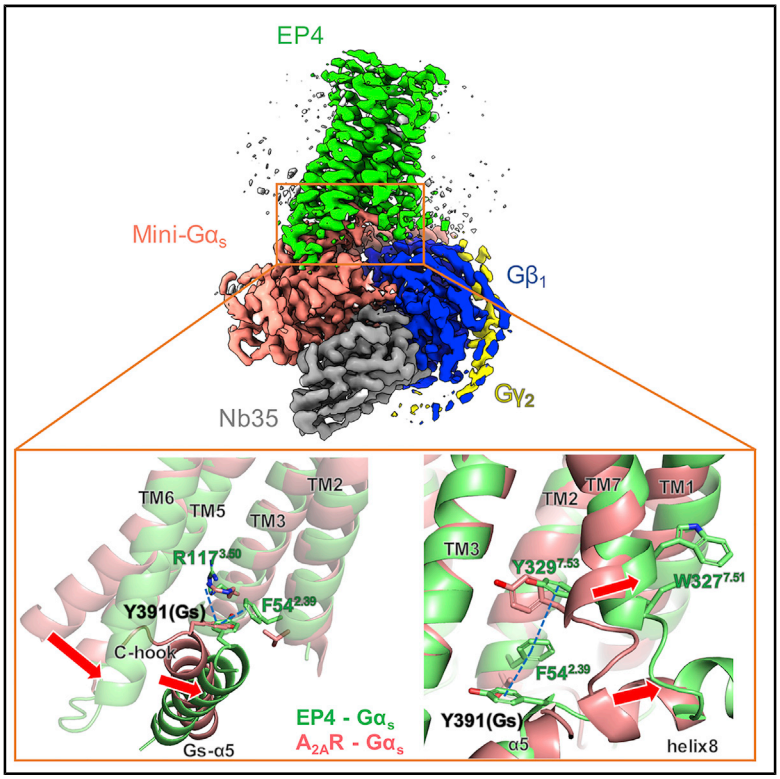

Highlights

- Cryo-EM structure of EP4-heterotrimeric G protein (Gs) complex with PGE_2 at 3.3 Å
- Compared with other class A GPCRs bound to Gs, TM6 was shifted smaller
- α5 helix of Gs was inserted toward TM2 of EP4 and the C-terminal hook was unwound
- Structure was formed by conserved residues in prostanoid receptors

Authors

Shingo Nojima, Yoko Fujita, Kanako Terakado Kimura, ..., So Iwata, Hideki Shigematsu, Takuya Kobayashi

Correspondence

hideki.shigematsu@riken.jp (H.S.), kobayatk@hirakata.kmu.ac.jp (T.K.)

In Brief

Nojima and Fujita et al. determined the cryo-EM structure of prostaglandin E receptor EP4 bound to the heterotrimeric G protein and the endogenous ligand PGE_2. The structure reveals the novel binding mode between GPCRs and Gs, which provides us the information for the structure-based activation mechanism of prostanoid receptors.

Nojima et al., 2021, Structure *29*, 1–9
March 4, 2021
https://doi.org/10.1016/j.str.2020.11.007

CellPress

Please cite this article in press as: Nojima et al., Cryo-EM Structure of the Prostaglandin E Receptor EP4 Coupled to G Protein, Structure (2020), https://doi.org/10.1016/j.str.2020.11.007

Structure

CellPress

Article

Cryo-EM Structure of the Prostaglandin E Receptor EP4 Coupled to G Protein

Shingo Nojima,[1,6] Yoko Fujita,[2,3,6] Kanako Terakado Kimura,[1] Norimichi Nomura,[1] Ryoji Suno,[1,4] Kazushi Morimoto,[1] Masaki Yamamoto,[5] Takeshi Noda,[2,3] So Iwata,[1] Hideki Shigematsu,[5,*] and Takuya Kobayashi[1,4,7,*]

[1]Department of Cell Biology, Graduate School of Medicine, Kyoto University, Kyoto, Kyoto 606-8501, Japan
[2]Laboratory of Ultrastructural Virology, Institute for Frontier Life and Medical Sciences, Kyoto University, Kyoto, Kyoto 606-8507, Japan
[3]Laboratory of Ultrastructural Virology, Division of Integrated Life Science, Graduate School of Biostudies, Kyoto University, Kyoto, Kyoto 606-8507, Japan
[4]Department of Medical Chemistry, Kansai Medical University, Hirakata, Osaka 573-1010, Japan
[5]RIKEN Spring-8 Center, Life Science Research Infrastructure Group, Sayo-gun, Hyogo 679-5148, Japan
[6]These authors contributed equally
[7]Lead Contact
*Correspondence: hideki.shigematsu@riken.jp (H.S.), kobayatk@hirakata.kmu.ac.jp (T.K.)
https://doi.org/10.1016/j.str.2020.11.007

SUMMARY

Prostaglandin E receptor EP4, a class A G protein-coupled receptor (GPCR), is a common drug target in various disorders, such as acute decompensated heart failure and ulcerative colitis. Here, we report the cryo-electron microscopy (cryo-EM) structure of the EP4-heterotrimeric G protein (Gs) complex with the endogenous ligand at a global resolution of 3.3 Å. In this structure, compared with that in the inactive EP4 structure, the sixth transmembrane domain is shifted outward on the intracellular side, although the shift is smaller than that in other class A GPCRs bound to Gs. Instead, the C-terminal helix of Gs is inserted toward TM2 of EP4, and the conserved C-terminal hook structure formsthe extended state. These structural features are formed by the conserved residues in prostanoid receptors (Phe54$^{2.39}$ and Trp327$^{7.51}$). These findings may be important for the thorough understanding of the G protein-binding mechanism of EP4 and other prostanoid receptors.

INTRODUCTION

Prostanoids are lipid mediators that are involved in various physiological processes, including inflammation, cardiovascular homeostasis, fertilization, and parturition (Hirata and Narumiya, 2011), and major prostanoids are metabolized from arachidonic acid. Cyclooxygenase oxidizes arachidonic acid to prostaglandin (PG) G_2, which is then reduced to PGH_2. Subsequently, PGH_2 is converted to PGD_2, PGE_2, $PGF_{2\alpha}$, PGI_2, or thromboxane A_2 by respective synthases. Prostanoid signals are transmitted via class A G protein-coupled receptors (GPCRs), namely, DP1, DP2, EP1, EP2, EP3, EP4, FP, IP, and TP (Hirata and Narumiya, 2011). These receptors are homologous, except for DP2, which is a member of the leukocyte chemoattractant family. EP1, EP2, EP3, and EP4 are all receptors for PGE_2, although the G proteins coupled to these receptors vary. Signaling assays have shown that EP1 is coupled to Gq, EP2, and EP4 are coupled to Gs, and EP3 is primarily coupled to Gi (Fujino and Regan, 2006; Inoue et al., 2019). G proteins transmit signals via different downstream signaling pathways. Gs, which is coupled to EP4, increases the concentration of cAMP by activating adenylyl cyclase.

EP4 is expressed in various tissues, including the thymus, ileum, lung, spleen, adrenal gland, and kidney (Bastien et al., 1994; Guan et al., 1996; Honda et al., 1993; Sando et al., 1994). As EP4 signaling is involved in carcinogenesis, cardiac hypertrophy, vasodilation, vascular remodeling, gastrointestinal homeostasis, renal function, and female reproductive function (Yokoyama et al., 2013), it is a candidate drug target for some diseases. Administration of EP4 agonist restored bone mass and strength in rats subjected to ovariectomy or immobilization, which normally cause loss of bone mass (Yoshida et al., 2002). This indicates that EP4 agonists can be potentially used as drugs for osteoporosis. The EP4 agonists ONO-4232, KAG-308, and CJ-023423 have been tested in clinical trials for acute decompensated heart failure, ulcerative colitis, and canine osteoarthritis, respectively (Rausch-Derra et al., 2016; Ward et al., 2016; Watanabe et al., 2015). In addition, the EP4 antagonist E7046 is in a phase I trial for anticancer agents (Bao et al., 2015).

Recent studies have revealed the structures of the active and inactive states of various lipid receptors, namely, lysophospholipid receptors ($S1P_1$, LPA_1, and LPA_6) (Chrencik et al., 2015; Hanson et al., 2012; Taniguchi et al., 2017), cannabinoid receptors (CB_1 and CB_2) (Hua et al., 2016, 2017, 2020; Kumar et al., 2019; Shao et al., 2016), leukotriene receptors ($cysLT_1$, $cysLT_2$, and BLT1) (Gusach et al., 2019; Hori et al., 2018; Luginina et al., 2019), prostanoid receptors (DP2, EP3, EP4, and TP) (Audet

Please cite this article in press as: Nojima et al., Cryo-EM Structure of the Prostaglandin E Receptor EP4 Coupled to G Protein, Structure (2020), https://doi.org/10.1016/j.str.2020.11.007

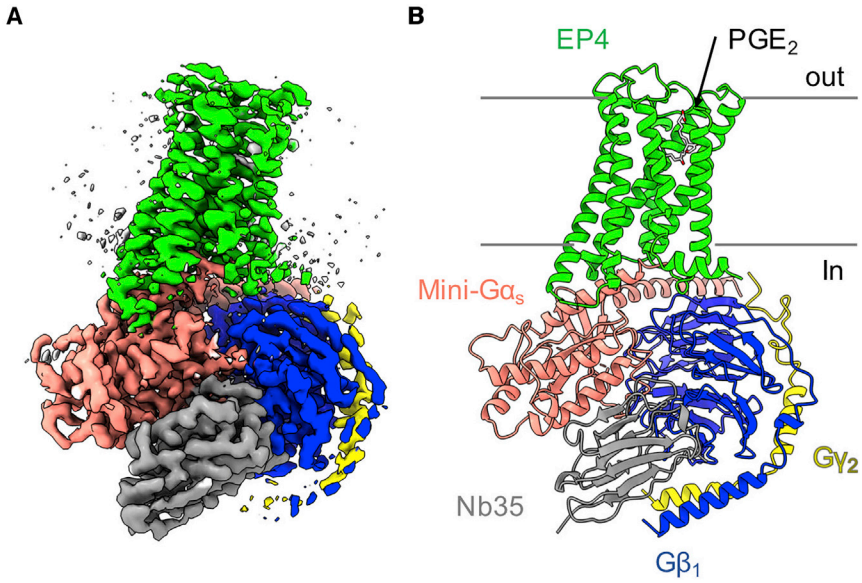

Figure 1. EM Map and 3D Model of the PGE_2-EP4-Gs$\beta_1\gamma_2$-Nb35 Complex

(A) The EM map of the EP4 complex at a resolution of 3.3 Å. The contour level of the map is set to 0.030 in order not to show the density of the micelle. The map derived from EP4, mini-Gs, Gβ_1, Gγ_2, and Nb35 is shown in green, light red, blue, yellow, and gray, respectively.

(B) The 3D model determined based on the EM map. The models are colored by chain as in (A). The gray stick indicates PGE_2.

See also Figures S1–S4.

et al., 2019; Fan et al., 2019; Morimoto et al., 2019; Toyoda et al., 2019; Wang et al., 2018), and platelet-activating factor receptor (Cao et al., 2018). Among these, structural information of the inactive form revealed common structural feature of lipid receptors. The extracellular loop 2 (ECL2) or N-terminal loop forms the lid structure and covers the ligand-binding pocket in many lipid receptors. Instead, large gaps exist on the transmembrane side through which the ligands are able to access the ligand-binding pocket in lipid receptors (Audet and Stevens, 2019). In particular, in EP4 and TP, gaps are observed between TM1 and TM7. The crystal structures of EP3 bound to the endogenous agonist PGE_2 or misoprostol-FA have been elucidated (Audet et al., 2019; Morimoto et al., 2019). In these agonist-bound structures, the gaps described above are closed. Based on this structural information, the helices forming the gap are thought to be flexible, and the gap appears to close after the agonist binds to the orthosteric ligand-binding site.

Structural features also exist at the receptor-G protein interface. GPCR activation generally proceeds in five steps: (1) the ligand binds to a GPCR on the extracellular side; (2) the conformation of the GPCR changes from an inactive to an active form; (3) conformational changes enable the heterotrimeric GDP-bound G protein (Gα, Gβ, and Gγ) to access the GPCR on the intracellular side; (4) GTP exchange occurs in the Ras-like GTPase domain of Gα; and (5) Gα and Gβ-Gγ heterodimers dissociate and transmit the signals to downstream factors (Gilman, 1987). Previous studies have successfully prepared stable GPCR-G protein complexes using GTP-free G protein to prevent the G protein from exchanging GTP and dissociating. Using these methods, the structures of β_1 and β_2 adrenergic receptors (β_1AR and β_2AR), adenosine A_{2A} receptor (A_{2A}R), and class A orphan GPCR (GPR52) have been determined to be class A GPCR-Gs complexes (García-Nafría et al., 2018; Lin et al., 2020; Rasmussen et al., 2011; Su et al., 2020; Zhang et al., 2020). Among these, the outward shift of the sixth transmembrane domain (TM6) of GPCR and insertion of the C-terminal helix of Gs into the GPCR are the structural features. At the residue level, the interaction between $Arg^{3.50}$ of the receptor and Tyr391 of Gs is the only common GPCR-Gs interaction. In addition, despite the absence of any conserved residue, TM3, intercellular loop 2 (ICL2), and TM5 interact with the C-terminal helix of Gs via hydrogen bonds and hydrophobic interactions, while TM6 interacts with the C-terminal loop (called the C-terminal hook) of Gs via hydrophobic interactions in these receptor-Gs complexes. The gap structure of lipid receptors and this activation feature of general GPCRs might be applicable to EP4. However, structural evidence of the active state EP4 is not available. Structural information regarding prostanoid receptor binding to G protein is also not available, because of which the coupling mechanism with G protein has not been revealed.

Here, we determined a cryoelectron microscopy (cryo-EM) structure of the PGE_2-EP4-Gs$\beta_1\gamma_2$-Nb35 complex at a resolution of 3.3 Å. This structure revealed not only the structural changes in EP4 when it transitions from the inactive state to the active state, but also the unique binding mode between GPCR and G protein which seems to be common in prostanoid receptors.

RESULTS

Cryo-EM Structure of the PGE_2-EP4-Gs$\beta_1\gamma_2$-Nb35 Complex

To prepare a stable EP4-Gs complex, EP4, mini-Gs, Gβ_1-Gγ_2 heterodimer, and nanobody (Nb35) (Rasmussen et al., 2011) were used. The expression construct of EP4 was essentially the same as that used in a previous crystallographic study (Toyoda et al., 2019), except that the two thermo-stabilizing point mutations $Ala62^{2.47}$Leu and $Gly106^{3.39}$Arg were not introduced, as these mutations shift the conformational equilibrium toward an inactive state and prevent PGE_2 binding. In brief, the human EP4 receptor was modified to add the signal sequence of hemagglutinin, followed by a FLAG epitope at the N terminus, and the His_8 tag at the C terminus, both flanked by the 3C cleavage site. The N-terminal residues (residues 1–3), C-terminal residues (residues 367–488), and ICL3 (residues 218–259) were deleted, and the N-linked glycosylation sites (Asn7 and Asn177) were mutated to glutamine. Using the signaling assay, it has been confirmed

Please cite this article in press as: Nojima et al., Cryo-EM Structure of the Prostaglandin E Receptor EP4 Coupled to G Protein, Structure (2020), https://doi.org/10.1016/j.str.2020.11.007

Table 1. Cryo-EM Data Collection, Refinement, and Validation Statistics

	PGE_2-EP4-Gs$\beta_1\gamma_2$-Nb35 Complex at 3.3 Å (EMDB: EMD-30608) (PDB: 7D7M)
Data Collection and Processing	
Magnification	105,000
Voltage (kV)	300
Electron exposure (e–/Å^2)	50.0
Defocus range (μm)	−0.6 ∼ −1.8
Pixel size (Å)	0.85
No. of initial particle images	2,796,263
No. of final particle images	178,217
Map resolution (Å)	3.3
FSC threshold	0.143
Map resolution range (Å)	3.13–4.26
Refinement	
Initial model used (PDB code)	6YWY (EP4) 6GDG (Gs, Gβ_1, Gγ_2, Nb35)
Model resolution (Å)	3.6
FSC threshold	0.5
Map sharpening B factor (Å^2)	−106.26
Model composition	7,326
Non-hydrogen atoms	1,031
Protein residues	1
Ligands	
B factors (Å^2)	
Protein	39.2
Ligand	89.0
RMSD	
Bond lengths (Å)	0.01
Bond angles (°)	0.98
Validation	
MolProbity score	1.5
Clashscore	9.6
Poor rotamers (%)	0.00
Ramachandran plot (%)	
Favored	98.7
Allowed	1.3
Disallowed	0.0

FSC, Fourier shell correlation; RMSD, root-mean-square deviation.

that the expression construct maintained Gs signaling (Toyoda et al., 2019). EP4 was purified and subsequently mixed with PGE_2, the mini-Gs heterotrimer (mini-Gs399 [García-Nafría et al., 2018], Gβ_1, and Gγ_2), and Nb35, which stabilizes the GPCR-Gs complex. Surplus components were removed using gel filtration (Figure S1).

Vitrified EP4 complexes were imaged by single-particle cryo-EM using a Titan Krios G3i microscope equipped with a K3 camera. Initially, 254,883 particles were used to calculate three-dimensional (3D) reconstruction with a global resolution of 3.4 Å. The first attempt at model building was performed based on this map. The initial 3D model of the EP4-Gs$\beta_1\gamma_2$-Nb35 complex can be generated using this map. To improve the signal-to-noise ratio at the binding site of EP4 and Gs, focused classification without alignment was performed with signal subtraction using the mask generated for the EP4-Gs interface fitted on the first map. One of the four 3D classes from 68.96% of total particles showed better representation of the density around the EP4-Gs interface in the refined 3D model by using particles, after reverting the signal (Figures 1A and S2). The global resolution of this map is reported to be 3.3 Å. On this map, the density isolated compared with the density of the protein appeared around the middle of TM1 and TM2 of EP4, and density that was not isolated but clearly extruded from the model of protein also appeared near the isolated density. When the crystal structure of EP3 bound to PGE_2 (Morimoto et al., 2019) was superposed on the initial 3D model of the EP4-Gs$\beta_1\gamma_2$-Nb35 complex, the isolated density overlapped with the five-membered carbon ring of PGE_2 and the extruded density overlapped with the alkyl side chain of the PGE_2, called the ω chain (Figure S3). Previous

Please cite this article in press as: Nojima et al., Cryo-EM Structure of the Prostaglandin E Receptor EP4 Coupled to G Protein, Structure (2020), https://doi.org/10.1016/j.str.2020.11.007

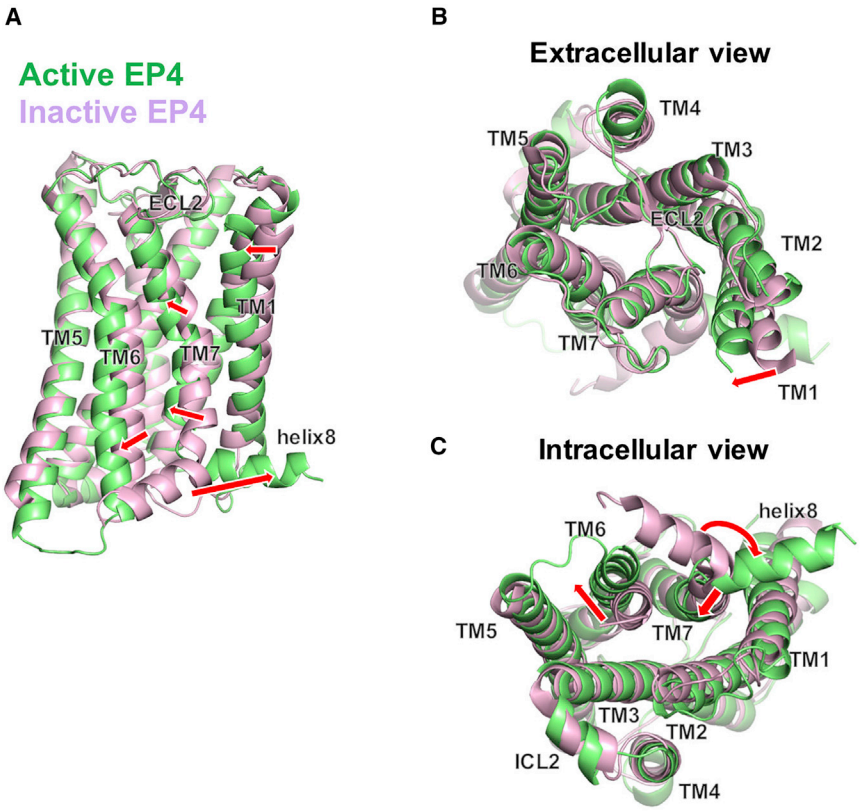

Figure 2. Structural Comparison between Active and Inactive EP4

(A) Side view, (B) extracellular view, and (C) intracellular view. Green and pink cartoons indicate the active and inactive EP4s (PDB: 5YWY), respectively. The conformational changes are shown by red arrows.

studies revealed that the residues of EP4 corresponding to the residues of EP3 bound to the carboxyl group of PGE_2 are also involved in PGE_2 binding, based on the binding assay (Morimoto et al., 2019; Toyoda et al., 2019), thus it could be speculated that the PGE_2-binding mode of EP4 is similar to that of EP3. Therefore, the PGE_2 model in the EP4-Gs$\beta_1\gamma_2$-Nb35 complex was initially built based on the crystal structure of PGE_2. The final 3D model of the PGE_2-EP4-Gs$\beta_1\gamma_2$-Nb35 complex was built and refined on the map with a global resolution of 3.3 Å (Figures 1B and S4; Table 1). The map allowed accurate placement of the residues in the regions of Ser19-Cys345 (except for ICL3) of EP4, Gln12-Gln59, Thr204-Asn254, and Arg265-Leu393 of Gs, and Asp5-Asn340 of Gβ_1, Gln11-Lys64 of Gγ_2, and Gln1-Ser128 of Nb35.

The active EP4 complex adopted the typical architecture of the activated class A GPCR conformation. Gs, Gβ_1, Gγ_2, and Nb35 formed a heterotetrameric complex, which exhibited almost the same structure as the Gs$\beta_1\gamma_2$-Nb35 complex bound to A_{2A}R (García-Nafría et al., 2018) (root-mean-square deviation = 0.876 Å for 669 Cα atoms). EP4 adopted an intracellular open state due to the outward shift of TM6. Similar to other activated class A GPCRs, EP4 and the Gs$\beta_1\gamma_2$-Nb35 complex formed a complex by the insertion of the C-terminal helix (α5) of Gs into the intracellular side of EP4.

Conformational Transition from an Inactive State to Active State of EP4

The 3D model of the active state EP4 was compared with the crystal structure of antagonist-bound EP4, previously determined to be an inactive state (Toyoda et al., 2019). There were four major conformational changes between the two structures (Figure 2). (1) Inactive EP4 harbored a gap between TM1 and TM7 on the extracellular side, which was closed in the active state EP4. (2) The TM6 of the active state EP4 was shifted toward the outside of the receptor on the intracellular side. (3) TM7 was attracted to the receptor on the middle and intracellular sides. These three differences are similar to the conformational changes observed upon transition from the inactive state to the active state of cannabinoid receptors (CB_1 and CB_2) (Hua et al., 2016, 2017, 2020; Kumar et al., 2019; Shao et al., 2016). (4) Compared with that of the inactive state EP4, helix 8 of the active state EP4 was extended in a different direction, with an angular difference of approximately 113°. The difference of helix 8 may be a crystallization artifact, as helix 8 was found to be involved in crystal packing in inactive EP4. Whether the difference of helix 8 is artifact or not, the conformational transition of TM1, TM6, TM7 of EP4 indicates that the conformational transition of EP4 from the inactive to the active state is typical of that of other lipid receptors.

PGE_2-Binding Site

The five-member carbon ring of PGE_2 was located around Met27$^{1.42}$, Thr69$^{2.54}$, and Ser73$^{2.58}$ (Figure 3A). The ω chain of PGE_2 was extended to the side pocket formed by helices TM3, TM5, and ECL2. The density of the carboxyl side chain of PGE_2, called an α chain, did not appear on the EM map, but the previous studies revealed that Tyr80$^{2.65}$, Thr168^{ECL2}, and R316$^{7.40}$ of EP4 were involved in PGE_2 binding by binding assay and these residues corresponded to the residues of EP3 bound to the carboxyl group of PGE_2 (Toyoda et al., 2019). Therefore, the α chain of PGE_2 was placed around TM1, TM2, TM7, and ECL2 on the extracellular side (Figure 3B). The residues related to signal activity were validated using the signaling assay with EP4 site-directed mutants. To evaluate Gs-signaling activity, the concentration of cAMP after adding PGE_2 in HEK293 cells was traced using the GloSensor cAMP assay (Promega). In this assay, the luminescence caused by the activation of cAMP-dependent luciferase was counted. Based on the results of this assay, the mutation of the residues at the orthosteric ligand-binding site, Phe24$^{1.39}$, Met27$^{1.42}$, Thr69$^{2.54}$, Ser73$^{2.58}$, Thr76$^{2.61}$, Tyr80$^{2.65}$, leu99$^{3.32}$, Ser103$^{3.36}$, Thr168^{ECL2},

Please cite this article in press as: Nojima et al., Cryo-EM Structure of the Prostaglandin E Receptor EP4 Coupled to G Protein, Structure (2020), https://doi.org/10.1016/j.str.2020.11.007

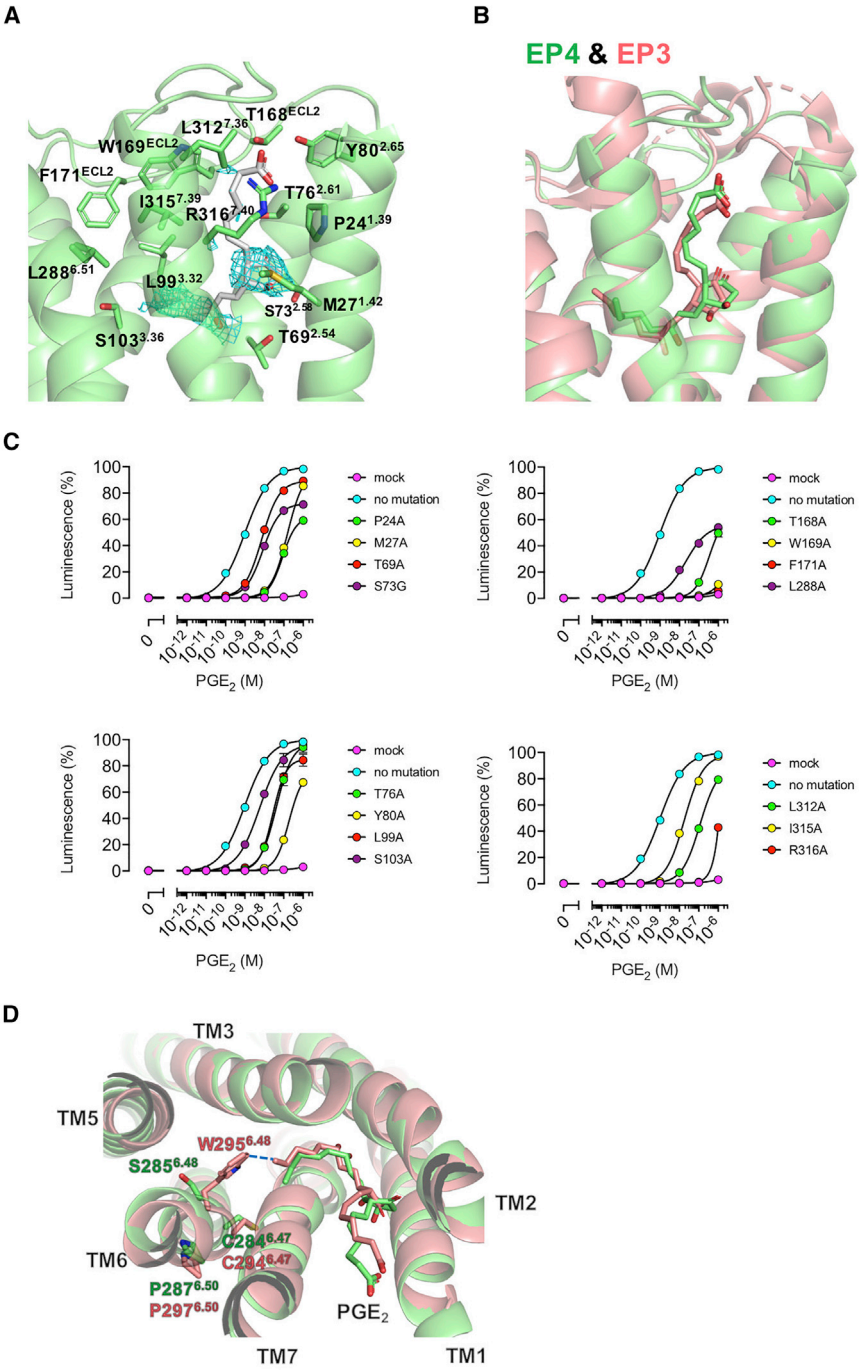

Figure 3. Ligand-Binding Site of EP4

(A) Residues of EP4 interacting with PGE_2. The side chains of EP4 and PGE_2 are shown as sticks. Green, EP4; gray, PGE_2. Cyan mesh indicates the density map around the PGE_2 model.

(B) Comparison of the positions of PGE_2 between EP4 (green) and EP3 (PDB: 6AK3) (light red).

(C) Signaling analysis of EP4 site-directed mutants using a GloSensor cAMP assay. The experiments were performed in triplicates (n = 3) and the error bars indicate the standard error of the mean (SEM).

(D) Comparison of the CWxP motif of EP4 (green) and EP3 (light red). See also Figures S3 and S5, and Table S1.

Trp169^{ECL2}, Phe171^{ECL2}, Leu288$^{6.51}$, Leu312$^{7.36}$, Ile315$^{7.39}$, and Arg316$^{7.40}$ decreased signal activity (Figure 3C; Table S1).

To compare the ligand-binding residues between EP4 and EP3, the crystal structure of EP3 bound to PGE_2 (PDB: 6AK3) (Morimoto et al., 2019) was superimposed on the 3D model of the PGE_2-EP4-Gs$\beta_1\gamma_2$-Nb35 complex. The position of PGE_2 in EP4 was similar to that of EP3, and the conformation of the transmembrane helices of EP4 were similar to those of EP3 (Figure S5). These results indicated that the carboxyl group of PGE_2 may form a salt bridge with R316$^{7.40}$ and hydrogen bonds with Tyr80$^{2.65}$ and Thr168^{ECL2}, and that the hydrophobic ω chain of PGE_2 was extended into the ligand-binding pocket, similar to that in EP3. The conformational similarity of EP3 and EP4 also indicated that PGE_2 interacted with TM1 and TM7 and closed the gap after entering the orthosteric ligand-binding site via the gap.

On the other hand, the ligand-binding sites of EP3 and EP4 at the generally conserved CWxP motif differed (Figure 3D). In many class A GPCRs, the CWxP motif is called the transmission switch (Trzaskowski et al., 2012). Trp$^{6.48}$ at the CWxP motif rotates when the ligand is bound to the receptor, triggering a large conformational change in TM6. Interestingly, EP4 contained Ser285$^{6.48}$ instead of the conserved Trp$^{6.48}$ in the transmission switch. The side chain of serine is small, which distances it from the ω chain end of PGE_2, whereas Trp$^{6.48}$ of EP3 is in contact with the ω chain end of PGE_2. The distinct residues that triggered the outward shift of TM6 were not detected; hence, we speculated that the spatial occlusion of TM7 bound and shifted by PGE_2 may cause a conformational change in TM6.

The EP4-Gsα Interface

In the 3D model of the EP4-Gs$\beta_1\gamma_2$-Nb35 complex, EP4 formed polar and nonpolar interactions with Gs, predominantly with the C-terminal α5 helix (α5) of Gs. Gs binds with TM1, TM2, TM3, TM5, TM6, TM7, ICL1, and ICL2 of EP4. The loop between the N-terminal helix (αN), the first β strand (β1), and the third and sixth β strands (β3 and β6) of Gs also interacted with EP4 (Figure 4A). In particular, His41 in the loop between αN and β1 formed a hydrogen bond with His129$^{34.55}$ of EP4. Phe219 in β3 of Gs formed π-π interactions with Tyr125$^{34.51}$ of EP4. Tyr358 in β6 of Gs formed cation-π interactions with Arg261$^{6.24}$ and hydrophobic interactions with Ile263$^{6.26}$. Tyr360 in β6 of Gs formed π-π interactions with Phe217$^{5.72}$, and cation-π interactions with

Please cite this article in press as: Nojima et al., Cryo-EM Structure of the Prostaglandin E Receptor EP4 Coupled to G Protein, Structure (2020), https://doi.org/10.1016/j.str.2020.11.007

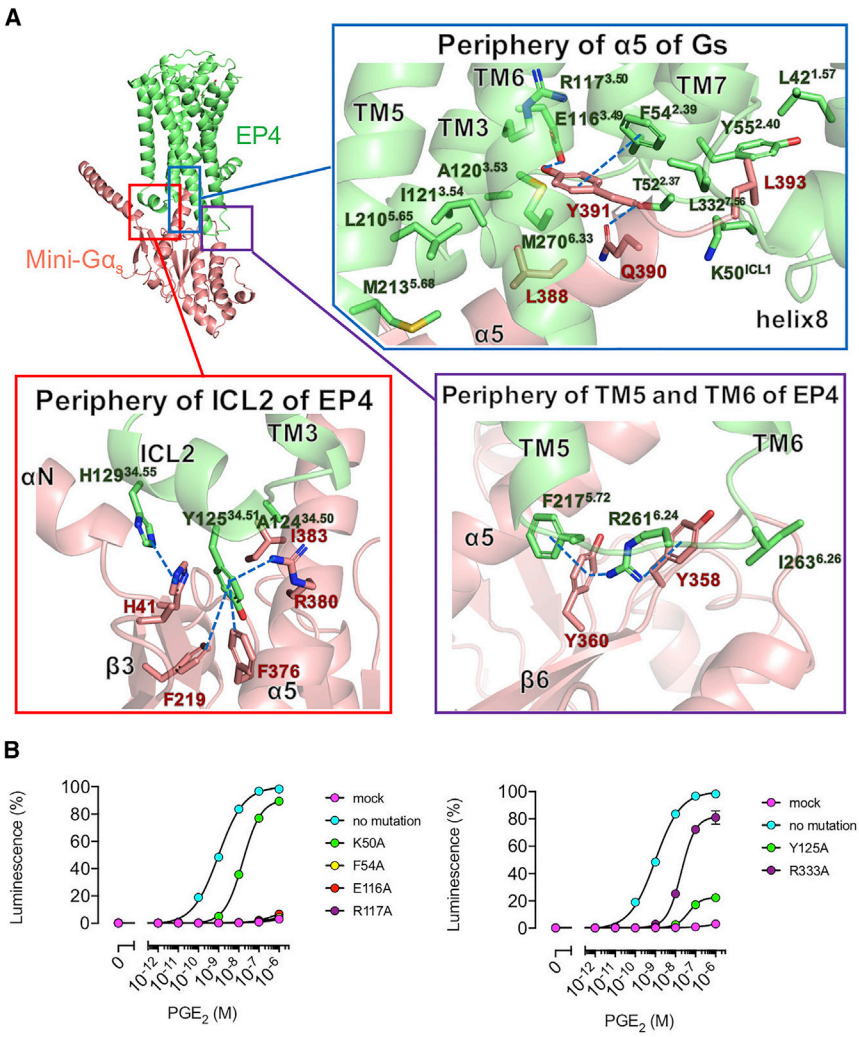

Figure 4. Interaction between EP4 and Gs

(A) Binding residues of EP4 with Gs. Green, EP4; pink, mini-Gs. Blue dashed lines indicate the interactions between residues.

(B) Signaling analysis of EP4 site-directed mutants using the GloSensor cAMP assay. The experiments were performed in triplicates (n = 3) and the error bars indicate SEM.

See also Table S1.

Arg261$^{6.24}$. The α5 of Gs widely interacted with TM2, TM3, ICL2, TM5, and TM6 of EP4 via π-π interactions (Phe376 with Tyr125$^{34.51}$, and Tyr391 with Phe54$^{2.39}$), cation-π interactions (Arg380 with Tyr125$^{34.51}$), hydrogen bonds (Gln390 with Thr52$^{2.37}$ and Tyr391 with Glu116$^{3.49}$), and many other hydrophobic interactions. The C-terminal loop of Gs (corresponding to the C-terminal hook) interacted with TM1, TM2, and TM7 via hydrophobic interactions.

These interactions were also validated using the GloSensor cAMP assay (Figure 4B; Table S1). The mutation of the residues around the EP4-Gs interface, Lys50^{ICL1}, Phe54$^{2.39}$, Glu116$^{3.49}$, Arg117$^{3.50}$, Tyr125$^{34.53}$, Leu274$^{6.37}$, and Arg333$^{8.47}$, decreased signal activity. Lys50^{ICL1} and Arg117$^{3.50}$ are relatively distant from Gs based on the EM structure, and the side chain of Arg333$^{8.47}$ was not modeled for the poor density on the map, although these residues were related to Gs signaling based on the signaling assay. Notably, critical residues for Gs signaling, Phe54$^{2.39}$, Glu116$^{3.49}$, and Arg117$^{3.50}$, are located near Tyr391 of Gs.

As described above, some structures of class A GPCR-Gs complexes had been determined. Compared with a representative of these structures, the cryo-EM structure of the A_{2A}R-Gs complex (PDB: 6GDG), the outward shift of the TM6 of EP4 was smaller than that of the other receptors (Figure 5A). Instead, the intracellular end of TM7 opened outward, leading to the outward arrangement of helix 8 (Figure 5B). Regarding binding with Gs, the interaction sites of EP4 with the C-terminal helix of Gs are almost the same as those of A_{2A}R, namely, TM3, ICL2, TM5, and TM6. However, the C-terminal hook of Gs did not interact with TM6. Instead, the hook was unwound and extended toward helix 8 (Figure 4A). Notably, EP4 had an extra interaction site at TM1, ICL1, and TM2 (Figure 5C). Phe54$^{2.39}$ on TM2 interacted with Tyr391 of Gs (Figure 5B). Phe54$^{2.39}$ is located not only near Tyr391 of Gs, but also near Tyr329$^{7.53}$. Tyr329$^{7.53}$ is a component of the N/DPxxY motif, which is one of the conserved motifs in class A GPCR. Tyr$^{7.53}$ of the N/DPxxY motif is known to relocate to the center of the receptor when the receptor is activated (Trzaskowski et al., 2012). However, Tyr329$^{7.53}$ of EP4 is located outside Tyr$^{7.53}$ of β_2AR or A_{2A}R. In addition, Trp327$^{7.51}$ is located at the outer surface of EP4. This large hydrophobic residue can interact with the hydrophobic residues of a neighbor helical pitch, such as Ile330$^{7.54}$, which bends the end of TM7 outside the receptor (Figure 5B). This conformational feature of TM7 maintains the space for the C terminus of Gs and allows the C-terminal hook of Gs to extend between TM1 and helix 8. The C-terminal hook structures were conserved in the GPCR-G protein complex, irrespective of the class of GPCR and type of G protein. Therefore, this is the first case in which the C-terminal hook formed an extended state when the G protein binds to GPCR.

DISCUSSION

In this study, we aimed to reveal the activation mechanism of EP4 by determining an EM structure of the PGE_2-EP4-Gs$\beta_1\gamma_2$-Nb35 complex. The cryo-EM structure of the PGE_2-EP4-Gs$\beta_1\gamma_2$-Nb35 complex revealed a unique binding mode and conformation of Gs. Two residues, Phe$^{2.39}$ and Trp$^{7.51}$, may characterize the conformation of the unique binding mode of prostanoid receptors. Compared with other class A GPCRs, the opening of TM6 of EP4 was smaller, and the C-terminal

Please cite this article in press as: Nojima et al., Cryo-EM Structure of the Prostaglandin E Receptor EP4 Coupled to G Protein, Structure (2020), https://doi.org/10.1016/j.str.2020.11.007

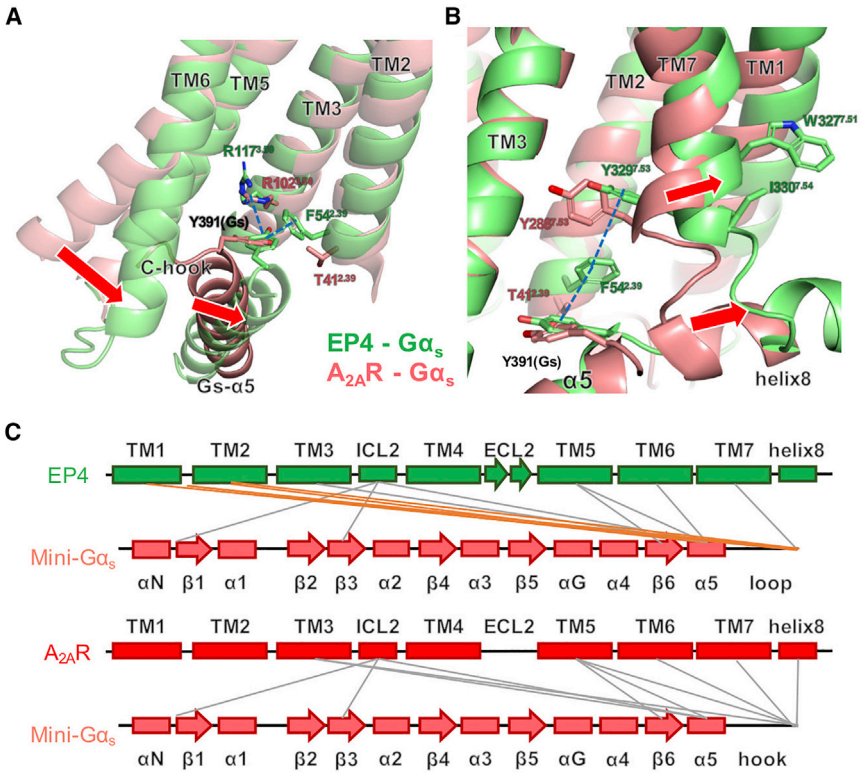

Figure 5. Structural Comparison of EP4 with Other Class A GPCR-Gs Complexes

(A) Structural comparison of the EP4-Gs complex and A_{2A}-Gs complex (PDB: 6GDG) around α5 of Gs and TM6 of GPCR. Green, EP4-Gs complex; pink, A_{2A}-Gs complex. The structural differences are shown by red arrows.

(B) Structural comparison of the intracellular side of TM7 and the unique residues of EP4. Color code is as in (A).

(C) Schematic diagram of the secondary structures of EP4, A_{2A}R, and mini-Gs. The boxes indicate α helices and arrows indicate β strands. Lines between diagrams indicate the interactions between GPCR and Gs. Orange lines indicate the unique interaction site in the EP4-mini-Gs complex.

hook formed an extended state. Owing to the steric hindrance with TM6, the α5 helix of Gs was inserted toward the TM2 of EP4. Based on the structural analysis and results of the signaling assay, $Phe^{2.39}$, $Glu^{3.49}$, and $Arg^{3.50}$ are located near Tyr391 of Gs and are necessary for Gs signaling. $Glu^{3.49}$ and $Arg^{3.50}$ are highly conserved in class A GPCRs. $Arg^{3.50}$ is commonly involved in the interaction of class A GPCRs with Gs. $Glu^{3.49}$ does not commonly interact with Gs; however, the difference in the α5 helix position allows interaction between $Glu^{3.49}$ and Tyr391 of Gs.

Furthermore, there are, besides prostanoid receptors, some class A GPCRs that have an aromatic side chain at residue 2.39. The relaxin receptors (RXFP1 and 2) and ADP receptors ($P2Y_{12}$, $P2Y_{13}$, and $P2Y_{14}$) also have Phe, His, or Tyr at residue 2.39. In addition, Tyr391 of Gs corresponds to Cys in Gi/Go, Tyr in Gq, and Ile in G12 (Nehmé et al., 2017); hence, at least Gi/Go and Gq may interact with $Phe^{2.39}$ via S-π or π-π interactions. Taken together, these receptors may also interact with G protein using a residue at the 2.39 position. $Phe^{2.39}$ also interacts with $Tyr329^{7.53}$ in the N/DPxxY motif and prevents TM7 from shifting inward in the receptor.

In addition, $Trp^{7.51}$ also opens TM7 outward on the intracellular side. $Trp^{7.51}$ is also conserved in prostanoid receptors. Besides prostanoid receptors, vasopressin receptors (V_{1A} and V_{1B}) are the other class A GPCRs that have tryptophan at residue 7.51. The C-terminal hook of the G protein coupled to these receptors may be extended as well as coupled to EP4.

This suggests that GPCRs of the same class have different critical residues for binding to G protein, and that solving the structure of individual GPCR-G protein complexes may be necessary to reveal the activation mechanism of each GPCR. In contrast, based on the sequence conservation and structural similarity of the active state structure of EP3, these structural features appear to be common in the prostanoid receptor family. Our findings should be applicable to the prostanoid receptors and some GPCRs that have the same unique residues, and they must strongly support studies regarding the activation mechanism of these receptors.

STAR★METHODS

Detailed methods are provided in the online version of this paper and include the following:

- KEY RESOURCES TABLE
- RESOURCE AVAILABILITY
  - Lead Contact
  - Materials Availability
  - Data and Code Availability
- EXPERIMENTAL MODEL AND SUBJECT DETAILS
  - Microbes
  - Cell Lines
- METHOD DETAILS
  - Construction, Expression, and Purification of EP4
  - Construction, Expression, and Purification of Mini-Gs399
  - Construction, Expression, and Purification of $G\beta_1$ and $G\gamma_2$
  - Construction, Expression, and Purification of Nb35
  - PGE_2-EP4-$Gs\beta_1\gamma_2$-Nb35 Complex Formation and Purification

- Cryo-EM Single Particle Analysis of the PGE_2-EP4-Gs$\beta_1\gamma_2$-Nb35 Complex
- Model Building and Refinement
- GloSensor cAMP Assay

● QUANTIFICATION AND STATISTICAL ANALYSIS

SUPPLEMENTAL INFORMATION

Supplemental Information can be found online at https://doi.org/10.1016/j.str.2020.11.007.

ACKNOWLEDGMENTS

This study was supported by JSPS KAKENHI grant no. JP19J12880 (to S.N.), AMED Core Research for Evolutional Science and Technology (CREST) under grant no. JP20gm0910007 (to T.K.), AMED Science and Technology Platform Program for Advanced Biological Medicine under grant no. JP20am0401020 (to T.K.), AMED Research on Development of New Drugs under grant no. JP20ak0101103 (to T.K., M.Y., H.S., and S.I.), Takeda Science Foundation (to T.K.), the Naito Foundation (to T.K.), Koyanagi Foundation (to T.K.), Private University Research Branding Project (to T.K.), AMED Basis for Supporting Innovative Drug Discovery and Life Science Research (BINDS) under grant no. JP20am0101079 (to S.I.), an AMED Research Program on Emerging and Re-emerging Infectious Disease grants under grant no. 19fk0108113 and 20fk0108270h0001 (to T.N.), and JSPS Core-to-Core Program A (to T.N.). This work was also supported in part by the RIKEN Dynamic Structural Biology project (to M.Y. and H.S.). We thank Drs. A. Tsutsumi, M. Kikkawa (Cryo-EM facility in the University of Tokyo, Tokyo, Japan) for their help in cryo-EM data collection. The cryo-EM data collection of this work was partially supported by AMED BINDS under grant no. JP19am0101115 (support no. 2365). DNA sequencing analysis was performed at the Medical Research Support Center, Graduate School of Medicine, Kyoto University. The manuscript was proofread by Editage (https://www.editage.jp/).

AUTHOR CONTRIBUTIONS

S.N., R.S., M.Y., T.N., S.I., H.S., and T.K. designed the project. S.N., R.S., and K.M. constructed the expression vector. S.N. expressed and purified the sample under the supervision of R.S. and N.N., and then Y.F., K.T.K., and H.S. prepared the sample grid, collected the cryo-EM images, and processed the EM data. S.N. built the 3D model. S.N. and K.M. designed and performed the GloSensor cAMP assay and analyzed the data. S.N. and Y.F. analyzed the data and compiled the figures for the manuscript. S.N. and H.S. wrote the manuscript. All authors discussed the results and commented on the manuscript.

DECLARATION OF INTERESTS

The authors declare no competing interests.

Received: October 7, 2020
Revised: October 27, 2020
Accepted: November 6, 2020
Published: December 1, 2020

REFERENCES

Adams, P.D., Afonine, P.V., Bunkóczi, G., Chen, V.B., Davis, I.W., Echols, N., Headd, J.J., Hung, L.W., Kapral, G.J., Grosse-Kunstleve, R.W., et al. (2010). PHENIX: a comprehensive Python-based system for macromolecular structure solution. Acta Crystallogr. Sect. D Biol. Crystallogr. *66*, 213–221.

Afonine, P.V., Poon, B.K., Read, R.J., Sobolev, O.V., Terwilliger, T.C., Urzhumtsev, A., and Adams, P.D. (2018). Real-space refinement in PHENIX for cryo-EM and crystallography. Acta Crystallogr. Sect. D Struct. Biol. *74*, 531–544.

Audet, M., and Stevens, R.C. (2019). Emerging structural biology of lipid G protein-coupled receptors. Protein Sci. *28*, 292–304.

Audet, M., White, K.L., Breton, B., Zarzycka, B., Han, G.W., Lu, Y., Gati, C., Batyuk, A., Popov, P., Velasquez, J., et al. (2019). Crystal structure of misoprostol bound to the labor inducer prostaglandin E_2 receptor. Nat. Chem. Biol. *15*, 11–17.

Bao, X., Albu, D., Huang, K.-C., Wu, J., Twine, N., Nomoto, K., and Woodall-Jappe, M. (2015). Combination of EP4 antagonist and checkpoint inhibitors promotes anti-tumor effector T cells in preclinical tumor models. J. Immunother. Cancer *3*, P350.

Bastien, L., Sawyer, N., Grygorczyk, R., Kathleen, M.M., and Adam, M. (1994). Cloning, functional expression, and characterization of the human prostaglandin E, receptor EP2 subtype. J. Biol. Chem. *269*, 11873–11877.

Cao, C., Tan, Q., Xu, C., He, L., Yang, L., Zhou, Y., Zhou, Y., Qiao, A., Lu, M., Yi, C., et al. (2018). Structural basis for signal recognition and transduction by platelet-activating-factor receptor. Nat. Struct. Mol. Biol. *25*, 488–495.

Carpenter, B., and Tate, C.G. (2016). Engineering a minimal G protein to facilitate crystallisation of G protein-coupled receptors in their active conformation. Protein Eng. Des. Sel. *29*, 583–593.

Chrencik, J.E., Roth, C.B., Terakado, M., Kurata, H., Omi, R., Kihara, Y., Warshaviak, D., Nakade, S., Asmar-Rovira, G., Mileni, M., et al. (2015). Crystal structure of antagonist bound human lysophosphatidic acid receptor 1. Cell *161*, 1633–1643.

Davis, I.W., Leaver-Fay, A., Chen, V.B., Block, J.N., Kapral, G.J., Wang, X., Murray, L.W., Arendall, W.B., Snoeyink, J., Richardson, J.S., et al. (2007). MolProbity: all-atom contacts and structure validation for proteins and nucleic acids. Nucleic Acids Res. *35*, 375–383.

Emsley, P., and Cowtan, K. (2004). Coot: model-building tools for molecular graphics. Acta Crystallogr. Sect. D Biol. Crystallogr. *60*, 2126–2132.

Fan, H., Chen, S., Yuan, X., Han, S., Zhang, H., Xia, W., Xu, Y., Zhao, Q., and Wu, B. (2019). Structural basis for ligand recognition of the human thromboxane A_2 receptor. Nat. Chem. Biol. *15*, 27–33.

Fujino, H., and Regan, J.W. (2006). EP 4 prostanoid receptor coupling to a pertussis toxin-sensitive inhibitory G protein. Mol. Pharmacol. *69*, 5–10.

García-Nafría, J., Lee, Y., Bai, X., Carpenter, B., and Tate, C.G. (2018). Cryo-EM structure of the adenosine A_{2A} receptor coupled to an engineered heterotrimeric G protein. eLife *7*, e35946.

Gilman, A.G. (1987). G proteins: transducers of receptor-generated signals. Annu. Rev. Biochem. *56*, 615–649.

Goddard, T.D., Huang, C.C., Meng, E.C., Pettersen, E.F., Couch, G.S., Morris, J.H., and Ferrin, T.E. (2018). UCSF ChimeraX: meeting modern challenges in visualization and analysis. Protein Sci. *27*, 14–25.

Guan, Y., Stillman, B.A., Zhang, Y., Schneider, A., Saito, O., Davis, L.S., Redha, R., Breyer, R.M., and Breyer, M.D. (1996). Cloning and expression of the rabbit prostaglandin EP4 receptor. Am. J. Physiol. *270*, F485–F493.

Gusach, A., Luginina, A., Marin, E., Brouillette, R.L., Besserer-Offroy, É., Longpré, J.M., Ishchenko, A., Popov, P., Patel, N., Fujimoto, T., et al. (2019). Structural basis of ligand selectivity and disease mutations in cysteinyl leukotriene receptors. Nat. Commun. *10*, 5573.

Hanson, M.A., Roth, C.B., Jo, E., Griffith, M.T., Scott, F.L., Reinhart, G., Desale, H., Clemons, B., Cahalan, S.M., Schuerer, S.C., et al. (2012). Crystal structure of a lipid G protein-coupled receptor. Science *335*, 851–855.

Hirata, T., and Narumiya, S. (2011). Prostanoid receptors. Chem. Rev. *111*, 6209–6230.

Honda, A., Sugimoto, Y., Namba, T., Watabe, A., Irie, A., Negishi, M., Narumiya, S., and Ichikawa, A. (1993). Cloning and expression of a cDNA for mouse prostaglandin E receptor EP2 subtype. J. Biol. Chem. *268*, 7759–7762.

Hori, T., Okuno, T., Hirata, K., Yamashita, K., Kawano, Y., Yamamoto, M., Hato, M., Nakamura, M., Shimizu, T., Yokomizo, T., et al. (2018). Na^+-mimicking ligands stabilize the inactive state of leukotriene B_4 receptor BLT1. Nat. Chem. Biol. *14*, 262–269.

Hua, T., Vemuri, K., Pu, M., Qu, L., Han, G.W., Wu, Y., Zhao, S., Shui, W., Li, S., Korde, A., et al. (2016). Crystal structure of the human cannabinoid receptor CB_1. Cell *167*, 750–762.e14.

Hua, T., Vemuri, K., Nikas, S.P., Laprairie, R.B., Wu, Y., Qu, L., Pu, M., Korde, A., Jiang, S., Ho, J.H., et al. (2017). Crystal structures of agonist-bound human cannabinoid receptor CB_1. Nature *547*, 468–471.

Hua, T., Li, X., Wu, L., Iliopoulos-Tsoutsouvas, C., Wang, Y., Wu, M., Shen, L., Johnston, C.A., Nikas, S.P., Song, F., et al. (2020). Activation and signaling mechanism revealed by cannabinoid receptor-Gi complex structures. Cell *180*, 655–665.e18.

Inoue, A., Ishiguro, J., Kitamura, H., Arima, N., Okutani, M., Shuto, A., Higashiyama, S., Ohwada, T., Arai, H., Makide, K., et al. (2012). TGFα shedding assay: an accurate and versatile method for detecting GPCR activation. Nat. Methods *9*, 1021–2029.

Inoue, A., Raimondi, F., Kadji, F.M.N., Singh, G., Kishi, T., Uwamizu, A., Ono, Y., Shinjo, Y., Ishida, S., Arang, N., et al. (2019). Illuminating G-protein-coupling selectivity of GPCRs. Cell *177*, 1933–1947.e25.

Kumar, K.K., Shalev-Benami, M., Robertson, M.J., Hu, H., Banister, S.D., Hollingsworth, S.A., Latorraca, N.R., Kato, H.E., Hilger, D., Maeda, S., et al. (2019). Structure of a signaling cannabinoid receptor 1-G protein complex. Cell *176*, 448–458.e12.

Lin, X., Li, M., Wang, N., Wu, Y., Luo, Z., Guo, S., Han, G.W., Li, S., Yue, Y., Wei, X., et al. (2020). Structural basis of ligand recognition and self-activation of orphan GPR52. Nature *579*, 152–157.

Luginina, A., Gusach, A., Marin, E., Mishin, A., Brouillette, R., Popov, P., Shiriaeva, A., Besserer-Offroy, É., Longpré, J.M., Lyapina, E., et al. (2019). Structure-based mechanism of cysteinyl leukotriene receptor inhibition by antiasthmatic drugs. Sci. Adv. *5*, 2518.

Morimoto, K., Suno, R., Hotta, Y., Yamashita, K., Hirata, K., Yamamoto, M., Narumiya, S., Iwata, S., and Kobayashi, T. (2019). Crystal structure of the endogenous agonist-bound prostanoid receptor EP3. Nat. Chem. Biol. *15*, 8–10.

Nehmé, R., Carpenter, B., Singhal, A., Strege, A., Edwards, P.C., White, C.F., Du, H., Grisshammer, R., and Tate, C.G. (2017). Mini-G proteins: novel tools for studying GPCRs in their active conformation. PLoS One *12*, e0175642.

Pettersen, E.F., Goddard, T.D., Huang, C.C., Couch, G.S., Greenblatt, D.M., Meng, E.C., and Ferrin, T.E. (2004). UCSF Chimera—a visualization system for exploratory research and analysis. J. Comput. Chem. *25*, 1605–1612.

Rasmussen, S.G.F., Devree, B.T., Zou, Y., Kruse, A.C., Chung, K.Y., Kobilka, T.S., Thian, F.S., Chae, P.S., Pardon, E., Calinski, D., et al. (2011). Crystal structure of the β_2 adrenergic receptor-Gs protein complex. Nature *477*, 549–555.

Rausch-Derra, L., Huebner, M., Wofford, J., and Rhodes, L. (2016). A prospective, randomized, masked, placebo-controlled multisite clinical study of grapiprant, an EP4 prostaglandin receptor antagonist (PRA), in dogs with osteoarthritis. J. Vet. Intern. Med. *30*, 756–763.

Rohou, A., and Grigorieff, N. (2015). CTFFIND4: fast and accurate defocus estimation from electron micrographs. J. Struct. Biol. *192*, 216–221.

Sando, T., Usui, T., Tanaka, I., Mori, K., Sasaki, Y., Fukuda, Y., Namba, T., Sugimoto, Y., Ichikawa, A., Narumiya, S., et al. (1994). Molecular cloning and expression of rat prostaglandin E receptor EP2 subtype. Biochem. Biophys. Res. Commun. *200*, 1329–1333.

Schorb, M., Haberbosch, I., Hagen, W.J.H., Schwab, Y., and Mastronarde, D.N. (2019). Software tools for automated transmission electron microscopy. Nat. Methods *16*, 471–477.

Shao, Z., Yin, J., Chapman, K., Grzemska, M., Clark, L., Wang, J., and Rosenbaum, D.M. (2016). High-resolution crystal structure of the human CB1 cannabinoid receptor. Nature *540*, 602–606.

Su, M., Zhu, L., Zhang, Y., Paknejad, N., Dey, R., Huang, J., Lee, M.-Y., Williams, D., Jordan, K.D., Eng, E.T., et al. (2020). Structural basis of the activation of heterotrimeric Gs-protein by isoproterenol-bound β_1-adrenergic receptor. Mol. Cell. *80*, 59–71.e4.

Taniguchi, R., Inoue, A., Sayama, M., Uwamizu, A., Yamashita, K., Hirata, K., Yoshida, M., Tanaka, Y., Kato, H.E., Nakada-Nakura, Y., et al. (2017). Structural insights into ligand recognition by the lysophosphatidic acid receptor LPA_6. Nature *548*, 356–360.

Toyoda, Y., Morimoto, K., Suno, R., Horita, S., Yamashita, K., Hirata, K., Sekiguchi, Y., Yasuda, S., Shiroishi, M., Shimizu, T., et al. (2019). Ligand binding to human prostaglandin E receptor EP4 at the lipid-bilayer interface. Nat. Chem. Biol. *15*, 18–26.

Trzaskowski, B., Latek, D., Yuan, S., Ghoshdastider, U., Debinski, A., and Filipek, S. (2012). Action of molecular switches in GPCRs—theoretical and experimental studies. Curr. Med. Chem. *19*, 1090–1109.

Wang, L., Yao, D., Deepak, R.N.V.K., Liu, H., Xiao, Q., Fan, H., Gong, W., Wei, Z., and Zhang, C. (2018). Structures of the human PGD_2 receptor CRTH2 reveal novel mechanisms for ligand recognition. Mol. Cell. *72*, 48–59.

Ward, C.L., Jamieson, V., Nabata, T., Sharpe, J., Dozono, K., Suto, F., Hashimoto, Y., and Gussak, I. (2016). First clinical experience with ONO-4232: a randomized, double-blind, placebo-controlled healthy volunteer study of a novel lusitropic agent for acutely decompensated heart failure. Clin. Ther. *38*, 1109–1121.

Watanabe, Y., Murata, T., Amakawa, M., Miyake, Y., Handa, T., Konishi, K., Matsumura, Y., Tanaka, T., and Takeuchi, K. (2015). KAG-308, a newly-identified EP4-selective agonist shows efficacy for treating ulcerative colitis and can bring about lower risk of colorectal carcinogenesis by oral administration. Eur. J. Pharmacol. *754*, 179–189.

Yokoyama, U., Iwatsubo, K., Umemura, M., Fujita, T., and Ishikawa, Y. (2013). The prostanoid EP4 receptor and its signaling pathway. Pharmacol. Rev. *65*, 1010–1052.

Yoshida, K., Oida, H., Kobayashi, T., Maruyama, T., Tanaka, M., Katayama, T., Yamaguchi, K., Segi, E., Tsuboyama, T., Matsushita, M., et al. (2002). Stimulation of bone formation and prevention of bone loss by prostaglandin E EP4 receptor activation. Proc. Natl. Acad. Sci. U S A *99*, 4580–4585.

Zhang, Y., Yang, F., Ling, S., Lv, P., Zhou, Y., Fang, W., Sun, W., Zhang, L., Shi, P., and Tian, C. (2020). Single-particle cryo-EM structural studies of the β_2AR-Gs complex bound with a full agonist formoterol. Cell Discov. *6*, 45.

Zivanov, J., Nakane, T., Forsberg, B.O., Kimanius, D., Hagen, W.J.H., Lindahl, E., and Scheres, S.H.W. (2018). New tools for automated high-resolution cryo-EM structure determination in RELION-3. Elife *7*, e42166.

Please cite this article in press as: Nojima et al., Cryo-EM Structure of the Prostaglandin E Receptor EP4 Coupled to G Protein, Structure (2020), https://doi.org/10.1016/j.str.2020.11.007

STAR★METHODS

KEY RESOURCES TABLE

REAGENT or RESOURCE	SOURCE	IDENTIFIER
Bacterial and Virus Strains		
Escherichia coli BL21-CodonPlus (DE3)-RIPL cells	Agilent Technologies	Cat# 230280
pFastBac baculovirus system	Invitrogen	Cat# 10359-016
BestBac 2.0, v-cath/chiA deleted baculovirus cotransfection system	Expression Systems	Cat# 91-002
Brevibacillus competent cells	Takara Bio	Cat# HB116
Chemicals, Peptides, and Recombinant Proteins		
Protease inhibitor cocktail	Nacalai Tesque	Cat# 25955-11
DDM (n-dodecyl-b-D-maltopyranoside), Sol-grade	Anatrace	Cat# D310S
Cholesterol hemi-succinate	Sigma	Cat# C6512
Colic acid sodium salt	Nacalai Tesque	Cat# 08805-56
Iodoacetamide	FujiFilm Wako Pure Chemical Corporation	Cat# 093-02892
Lauryl maltose neopentyl glycol (MNG)	Anatrace	Cat# NG310 25 GM
GDN	Anatrace	Cat# GDN101 25 GM
ONO-AE3-208	Cayman	Cat# 14522
PGE_2	Cayman	Cat# 14010
PF-04418948	Funakoshi	Cat# 15016
Apyrase	NEB	Cat# M0398L
D-luciferin	FujiFilm Wako Pure Chemical Corporation	Cat# 127-03941
Critical Commercial Assays		
GloSensor™ cAMP assay	Promega	Cat# E2301
Deposited data		
PGE_2-EP4-Gs$\beta_1\gamma_2$-Nb35 complex map	This paper	EMDB EMD-30608
PGE_2-EP4-Gs$\beta_1\gamma_2$-Nb35 complex model	This paper	PDB 7D7M
Crystal structure of EP4	(Toyoda et al., 2019)	PDB 5YWY
Crystal structure of EP3	(Morimoto et al., 2019)	PDB 6AK3
Cryo-EM structure of $A_{2A}R$	(García-Nafría et al., 2018)	PDB 6GDG
Experimental Models: Cell Lines		
Spodoptera frugiperda 9 (Sf9) insect cells	Thermo Fisher Scientific	Cat# 11496-015
Human embryonic kidney 293 (HEK293) cells	(Inoue et al., 2012)	N/A
Recombinant DNA		
pFastBac1-EP4-GFP	This paper	N/A
pET21a-mini-Gs399	This paper	N/A
pVL1393-Gβ_1-Gγ_2	This paper	N/A
pNY326-Nb35	This paper	N/A
pcDNA3.1-EP4	This paper	N/A
pGloSensor-22F cAMP Plasmid	Promega	Cat# E2301

(*Continued on next page*)

Please cite this article in press as: Nojima et al., Cryo-EM Structure of the Prostaglandin E Receptor EP4 Coupled to G Protein, Structure (2020), https://doi.org/10.1016/j.str.2020.11.007

Continued

REAGENT or RESOURCE	SOURCE	IDENTIFIER
Software and Algorithms		
SerialEM	(Schorb et al., 2019)	https://bio3d.colorado.edu/SerialEM/
RELION 3.0.8 and 3.1 beta	(Zivanov et al., 2018)	https://www3.mrc-lmb.cam.ac.uk/relion/index.php/Main_Page
CTFFIND4	(Rohou and Grigorieff, 2015)	https://grigoriefflab.umassmed.edu/ctffind4
Chimera version 1.14	(Pettersen et al., 2004)	https://www.cgl.ucsf.edu/chimera/
ChimeraX version: 1.0rc202005180441 (2020-05-18)	(Goddard et al., 2018)	https://www.cgl.ucsf.edu/chimerax/
COOT v0.8.9.2	(Emsley and Cowtan, 2004)	https://strucbio.biologie.unikonstanz.de/ccp4wiki/index.php/Coot
Phenix v1.18-3845-000	(Adams et al., 2010)	https://www.phenix-online.org/
phenix.real_space_refine	(Afonine et al., 2018)	https://www.phenix-online.org/
MolProbity	(Davis et al., 2007)	https://www.phenix-online.org/
Pymol	Schrödinger	http://www.pymol.org
Prism 8	GraphPad Software	https://www.graphpad.com/scientific-software/prism/
Other		
Ni-NTA resin	Qiagen	Cat# 30250
FLAG M1 affinity resin	Sigma	Cat# A4596-25ML
Amicon Ultra-15 centrifugal filter units 50,000 MWCO	Millipore	Cat# UFC905096
Amicon Ultra-15 centrifugal filter units 10,000 MWCO	Millipore	Cat# UFC901096
Amicon Ultra-4 centrifugal filter units 50,000 MWCO	Millipore	Cat# UFC805096
Superdex 200 Increase 10/300 GL	GE Healthcare	Cat# 28990944
PSFM-J1 medium	FujiFilm Wako Pure Chemical Corporation	Cat# 160-25851
Fetal bovine serum	Sigma	Cat# 172012-500ML
Dulbecco's modified Eagle's medium	Sigma	Cat# D6046-500ML
HBSS, calcium, magnesium, no phenol red	Gibco	Cat# 14025076
Quantifoil grid of R0.6/R1.0 300 mesh copper	Quantifoil	Cat# Q325CR-06

RESOURCE AVAILABILITY

Lead Contact

Further information and requests for resources and reagents should be directed to and will be fulfilled by the lead contact, Takuya Kobayashi (kobayatk@hirakata.kmu.ac.jp)

Materials Availability

This study did not generate new unique reagents.

Data and Code Availability

The cryo-EM reconstructions generated in this study have been deposited into the Electron Microscopy Data Bank with accession numbers EMDB: EMD-30608. The 3D models reported in this paper have been deposited in the Protein Data Bank with accession code PDB: 7D7M. All other data are available from the corresponding authors on reasonable request.

Please cite this article in press as: Nojima et al., Cryo-EM Structure of the Prostaglandin E Receptor EP4 Coupled to G Protein, Structure (2020), https://doi.org/10.1016/j.str.2020.11.007

EXPERIMENTAL MODEL AND SUBJECT DETAILS

Microbes

Escherichia coli BL21-CodonPlus (DE3)-RIPL cells (Agilent Technologies) were cultivated in terrific broth (TB) supplemented with 100 mg/L ampicillin at 37°C. *Brevibacillus* competent cells were cultivated in 2SY medium supplemented with 50 mg/L neomycin at 30°C. *Spodoptera frugiperda* 9 (Sf9) insect cells were cultured in PSFM-J1 medium (Wako) supplemented with 2% fetal bovine serum (FBS) (Sigma), 50 units/mL penicillin, 50 μg/mL streptomycin (Wako), and 0.5 μg/mL amphotericin B at 27°C.

Cell Lines

Human embryonic kidney 293 (HEK293) cells were grown in Dulbecco's modified Eagle's medium supplemented with 10% FBS (Sigma-Aldrich), 100 units/mL penicillin, and 100 μg/mL streptomycin (Wako) at 37°C in a 5% CO_2 incubator.

METHOD DETAILS

Construction, Expression, and Purification of EP4

The sequence of human EP4 was inserted into the Sf9 expression vector, pFastBac1 (Thermo Fisher Scientific). The N-terminal residues (residues 1–3), C-terminal residues (residues 347–488), and intracellular loop 3 (residues 218–259) were deleted, and N-linked glycosylation sites (Asn7 and Asn177) were mutated to glutamine. In addition, the hemagglutinin signal sequence, FLAG tag, and 3C protease cleavage site were added to the N-terminus, and the 3C cleavage site and GFP sequence were added to the C-terminus. This plasmid was named pFastBac1-EP4-GFP.

Recombinant baculovirus was obtained using the Bac-to-Bac baculovirus expression system (Invitrogen). Sf9 insect cells were cultured in a PSFM-J1 medium (Wako) supplemented with 2% FBS (Sigma-Aldrich), 50 units/mL penicillin, 50 μg/mL streptomycin, and 0.5 μg/mL amphotericin B. After the cell density reached 3.5×10^6, the Sf9 cells were infected with the baculovirus at a multiplicity of infection (M.O.I.) of 2 and cultivated at 27°C for 3 days. The cells were harvested via centrifugation at 7,000 × *g* for 10 min and re-harvested via centrifugation at 8,000 × *g* for 10 min after washing with phosphate-buffered saline (PBS) (-). The cells were suspended in 80% glycerol and stored at −80°C.

The cells were lysed in buffer A (10 mM HEPES [pH 7.5], 20 mM KCl, 10 mM $MgCl_2$, 1 μM ONO-AE3-208, and protease inhibitor cocktail). The suspension was homogenized with a dounce homogenizer and ultracentrifuged at 140,000 × *g* for 30 min at 4°C. The precipitate was suspended in buffer B (10 mM HEPES [pH 7.5], 1 M NaCl, 20 mM KCl, 1 μM ONO-AE3-208, and protease inhibitor cocktail) and ultracentrifuged at 140,000 × *g* for 30 min at 4°C. The precipitate was resuspended in buffer C (30 mM HEPES [pH 7.5], 750 mM NaCl, 5 mM imidazole, 1 mg/mL iodoacetamide, 1% n-dodecyl-β-D-maltoside [DDM], 0.2% cholesteryl hemisuccinate [CHS], 0.2% sodium cholate, 10 μM ONO-AE3-208, and protease inhibitor cocktail), and stirred gently at 4°C for 2 h. The insoluble components were removed via ultracentrifugation at 140,000 × *g* for 30 min at 4°C.

The supernatant was mixed with Ni-NTA resin (Qiagen) and stirred gently overnight at 4°C. The resin was washed with 11 column volumes of buffer D (30 mM HEPES [pH 7.5], 750 mM NaCl, 5 mM imidazole, 0.02% sodium cholate, 0.1% DDM, 0.03 % CHS, and 10 μM ONO-AE3-208). EP4 was eluted in five column volumes of buffer E (30 mM HEPES [pH 7.5], 750 mM NaCl, 500 mM imidazole, 0.02% sodium cholate, 0.1% DDM, 0.03% CHS, and 10 μM ONO-AE3-208). $CaCl_2$ (2 mM) was added to the eluted sample and loaded onto a FLAG M1 affinity resin (Sigma-Aldrich) equilibrated in buffer F (30 mM HEPES [pH 7.5], 750 mM NaCl, 3 mM $CaCl_2$, 0.02% sodium cholate, 0.1% DDM, 0.03% CHS, and 10 μM ONO-AE3-208). Buffer F loaded on the resin was gradually replaced with buffer G (30 mM HEPES [pH 7.5], 750 mM NaCl, 3 mM $CaCl_2$, 0.2% lauryl maltose neopentyl glycol [MNG], 0.02% CHS, and 10 μM ONO-AE3-208). EP4 was eluted with two column volumes of buffer H (20 mM HEPES [pH 7.5], 100 mM NaCl, 0.01% MNG, 0.001% CHS, 10 μM ONO-AE3-208, 5 mM EDTA, and 0.2 mg/mL FLAG peptide) and two column volumes of buffer I (20 mM HEPES [pH 7.5], 100 mM NaCl, 0.01 % MNG, 0.001 % CHS, 10 μM ONO-AE3-208, and 5 mM EDTA). The collected sample was supplemented with 100 μM ONO-AE3-208 and 3C protease and then stirred gently overnight at 4°C. The amount of 3C protease was 30 μg per mg sample protein. The sample was concentrated with Amicon Ultra-15 centrifugal filter units of 50,000 MWCO (Millipore) to 1 mL. The sample was further purified via gel filtration on a Superdex 200 Increase 10/300 GL (GE Healthcare) with buffer J (20 mM HEPES [pH 7.5], 100 mM NaCl, 0.01% MNG, 0.001% CHS, and 10 μM PGE_2).

Construction, Expression, and Purification of Mini-Gs399

The DNA sequence of mini-Gs399 was synthesized based on the amino acid sequence of mini-Gs399, as reported previously (Carpenter and Tate, 2016), but the residue corresponding to Leu63 of Gs was mutated to the tyrosine from the original sequence of mini-Gs399. The mini-Gs399 sequence was inserted into pET21a (Novagen). In this construct, the N-terminal 6 × His tag and TEV protease cleavage site were added to mini-Gs399. This plasmid is referred to as pET21a-mini-Gs399 in this study.

The plasmid was introduced into *E. coli* BL21-CodonPlus (DE3)-RIPL (Agilent Technologies). The cells were cultivated in TB supplemented with 100 mg/L ampicillin at 37°C. After the optical density (OD) of the broth at 600 nm wavelength reached 0.6, 500 μM isopropyl β-D-1-thiogalactopyranoside (IPTG) was added and incubated overnight at 25°C. The cells were harvested via centrifugation at 5,000 × *g* for 15 min and stored at −80°C. The purification of mini-Gs399 was performed according to García-Nafría et al. (2018). The cells were suspended in buffer K (40 mM HEPES [pH7.5], 100 mM NaCl, 10% glycerol, 10 mM imidazole, 5 mM $MgCl_2$, 50 μM GDP, 25 U/L DNase I, and protease inhibitor cocktail) and lysed via sonication (70 % amplitude, 1 s ON 1.5 s OFF,

Please cite this article in press as: Nojima et al., Cryo-EM Structure of the Prostaglandin E Receptor EP4 Coupled to G Protein, Structure (2020), https://doi.org/10.1016/j.str.2020.11.007

10 min). The insoluble components were removed via centrifugation at 40,000 × *g* for 45 min. The supernatant was loaded onto a Ni Sepharose FF resin column (GE Healthcare). The resin was washed with 10 column volumes of buffer L (20 mM HEPES [pH7.5], 500 mM NaCl, 10% glycerol, 40 mM imidazole, 1 mM $MgCl_2$, and 50 μM GDP), and the resin-binding protein was eluted in 3 column volumes of buffer M (20 mM HEPES [pH7.5], 100 mM NaCl, 10% glycerol, 500 mM imidazole, 1 mM $MgCl_2$, and 50 μM GDP). Dithiothreitol (DTT) (1 mM) and TEV protease were added to the eluate. The amount of TEV protease was 50 μg per mg sample protein. Then, the eluate was dialyzed overnight against buffer N (20 mM HEPES [pH7.5], 100 mM NaCl, 10 % glycerol, 1 mM $MgCl_2$, 10 μM GDP) at 4°C. Imidazole (20 mM) and Ni-NTA resin (Qiagen) were added to remove the resin-binding contaminant. The flow-through was collected. The resin was washed with 2.5 column volumes of buffer N and the flow-through was collected. The collected sample was concentrated with Amicon Ultra-15 centrifugal filter units of 10,000 MWCO (Millipore) to 5 mL. The sample was further purified via gel filtration using a HiLoad 16/600 Superdex 200 pg (GE Healthcare) with buffer O (10 mM HEPES [pH 7.5], 100 mM NaCl, 10% glycerol, 1 mM $MgCl_2$, 10 μM GDP, and 0.1 mM Tris [2-carboxyethyl] phosphine hydrochloride [TCEP]).

Construction, Expression, and Purification of $G\beta_1$ and $G\gamma_2$

The DNA sequences of $G\beta_1$ and $G\gamma_2$ were inserted into the multi-cloning site of pFastBac Dual, which was then re-inserted in pVL1393. This plasmid is referred to as pVL1393-$G\beta_1$-$G\gamma_2$.

Recombinant baculovirus was produced using the BestBac 2.0, v-cath/chiA deleted baculovirus cotransfection system (Expression Systems). Sf9 insect cells were cultured in PSFM-J1 medium supplemented with 2% FBS, 50 units/mL penicillin, 50 μg/mL streptomycin, and 0.5 μg/mL amphotericin B. After the cell density reached 3.5 × 10^6, the Sf9 cells were infected with the baculovirus at M.O.I. of 2 and cultivated at 27°C for 3 days. The cells were harvested via centrifugation at 7,000 × *g* for 10 min and re-harvested via centrifugation at 8,000 × *g* for 10 min after washing with PBS (-). The cells were suspended in 80% glycerol and stored at −80°C.

The cells were lysed in buffer P (10 mM Tris [pH 7.5], 20 mM KCl, 0.1 mM $MgCl_2$, 10 mM 2-mercaptoethanol, 10 μM GDP, 1 mM benzamidine, and 2.5 μM leupeptine). The suspension was homogenized with a dounce homogenizer and ultracentrifuged at 177,000 × *g* for 30 min at 4°C. The precipitate was suspended in buffer Q (10 mM HEPES [pH 7.5], 1 M NaCl, 20 mM KCl, 10 mM $MgCl_2$, 10 mM 2-mercaptoethanol, 10 μM GDP, 1 mM benzamidine, and 2.5 μM leupeptine), and ultracentrifuged at 177,000 × *g* for 15 min at 4°C. The precipitate was resuspended in buffer R (20 mM HEPES [pH 7.5], 100 mM NaCl, 5 mM $MgCl_2$, 0.05% DDM, 1% sodium cholate, 10 mM 2-mercaptoethanol, 10 μM GDP, 1 mM benzamidine, and 2.5 μM leupeptine), and stirred gently at 4°C for 1 h. The insoluble components were removed via ultracentrifugation at 177,000 × *g* for 30 min at 4°C. Imidazole (20 mM) and Ni-NTA resin were added to the supernatant and stirred gently overnight at 4°C. The resin was washed with 16 column volumes of buffer S (20 mM HEPES [pH 7.5], 100 mM NaCl, 5 mM $MgCl_2$, 0.05% DDM, 1% sodium cholate, 10 mM 2-mercaptoethanol, and 10 μM GDP). Buffer S loaded on the resin was gradually replaced with buffer T (20 mM HEPES [pH 7.5], 100 mM NaCl, 1 mM $MgCl_2$, 0.05% DDM, 5 mM 2-mercaptoethanol, and 10 μM GDP). The resin was suspended in buffer T supplemented with 20 mM imidazole and 3C protease, and then stirred gently overnight at 4°C. The flow-through was collected. The resin was washed with 5 column volumes of buffer T and the flow-through was collected. The collected sample was concentrated with Amicon Ultra-15 centrifugal filter units of 50,000 MWCO (Millipore) to 1.5 mL. The sample was further purified via gel filtration on a Superdex 200 Increase 10/300 GL (GE Healthcare) with buffer U (20 mM HEPES [pH 7.5], 100 mM NaCl, 0.01 % MNG, 0.001 % CHS, and 0.1 mM TCEP).

Construction, Expression, and Purification of Nb35

The DNA sequence of Nb35 was synthesized based on the amino acid sequence of Nb35 (Rasmussen et al., 2011). The Nb35 sequence was inserted in pNY326. Sec signal peptide sequence was added at the N-terminus, and the TEV protease cleavage site, 6 × His tag, and HA tag were added at the C-terminus. This plasmid is referred to as pNY326-Nb35 in this study.

The plasmid was introduced into *Brevibacillus* competent cells (Takara Bio). The cells were cultivated in 2SY medium supplemented with 50 mg/L neomycin at 30°C for two days. The cells were removed via centrifugation at 6,000 × *g* for 15 min.

The supernatant was supplemented with 60 % ammonium sulfate and stirred at 4°C for 1 h, following which it was centrifuged at 10,000 × *g* for 20 min at 4°C. The precipitate was dissolved in Tris-buffered saline (TBS) and dialyzed overnight against TBS at 4°C. The sample was centrifuged at 15,000 × *g* for 5 min at 4°C. The supernatant was supplemented with 10 mM imidazole and Ni-NTA resin and stirred gently at 4°C for 1.5 hour. The resin was transferred to an empty column and washed with 10 column volumes of buffer V (10 mM Tris [pH 7.5], 150 mM NaCl, and 20 mM imidazole). The resin-binding protein was eluted in two column volumes of buffer W (10 mM Tris [pH 7.5], 150 mM NaCl, and 250 mM imidazole). The eluted fractions were supplemented with 9 mg TEV protease and dialyzed overnight against buffer X (20 mM Tris [pH 7.5], 150 mM NaCl) at 4°C. The sample was supplemented with 10 mM imidazole and centrifuged at 15,000 × *g* for 10 min at 4°C. The supernatant was loaded onto a HisTrap HP column (GE Healthcare) and the flow-through fraction was collected. The column was washed with three column volumes of buffer Y (10 mM Tris [pH 7.5], 150 mM NaCl, and 10 mM imidazole) and the wash fractions were also collected. The collected fractions were concentrated using Amicon Ultra-15 centrifugal filter units of 10,000 MWCO (Millipore) to 5 mL. The sample was further purified via gel filtration using a HiLoad 16/600 Superdex 200 pg (GE Healthcare) with TBS.

PGE_2-EP4-Gs$\beta_1\gamma_2$-Nb35 Complex Formation and Purification

Purified EP4, mini-Gs399, $G\beta_1$-$G\gamma_2$, and Nb35 were mixed at the molar ratio of 1: 1.2: 1.2: 2. The mixture was supplemented with 100 μM PGE_2, 0.1 U apyrase, 0.0033 % GDN, and 0.0013 % CHS, and then incubated overnight at 4°C. The sample was

Please cite this article in press as: Nojima et al., Cryo-EM Structure of the Prostaglandin E Receptor EP4 Coupled to G Protein, Structure (2020), https://doi.org/10.1016/j.str.2020.11.007

concentrated with Amicon Ultra-15 centrifugal filter units of 50,000 MWCO (Millipore) to 0.5 mL. The sample was further purified via gel filtration on a Superdex 200 Increase 10/300 GL (GE Healthcare) with buffer Z (10 mM HEPES [pH 7.5], 100 mM NaCl, 0.00075% MNG, 0.00025% GDN, 0.000125% CHS, and 10 μM PGE_2). The purified complex was concentrated with Amicon Ultra-4 centrifugal filter units of 50,000 MWCO (Millipore) to 8.4 mg/mL (approximately 70 μM).

Cryo-EM Single Particle Analysis of the PGE_2-EP4-Gs$\beta_1\gamma_2$-Nb35 Complex

A holey carbon grid, Quantifoil grid of R0.6/R1.0 300 mesh copper (Quantifoil), was glow-discharged at 7 Pa with 10 mA for 10 s using a JEC-3000FC sputter coater (JEOL) prior to use. A 3-μL aliquot was applied onto the grid, blotted for 3.5 s with BlotForce of +10 in 100% humidity at 8°C, and plunged into liquid ethane using a VitrobotMkIV (Thermo Fisher Scientific). Cryo-EM data collection for screening sample quality and grid conditions was performed using Glacios (Thermo Fisher Scientific) at 200 kV with a Falcon3EC direct electron detector in the counting mode at the RIKEN RSC Cryo-EM facility (Hyogo, Japan). After several screening sessions, data were collected on an optimized grid using a Titan Krios G3i (Thermo Fisher Scientific) operated at 300 kV, equipped with a BioQuantum energy filter in zero-loss EFTEM NanoProbe mode with a 25 eV energy selection slit and K3 direct electron detector (Gatan) in counting mode at the Cryo-EM Facility of the University of Tokyo (Tokyo, Japan). Movie stacks were acquired at 105,000× nominal magnification, with an accumulated dose of 50.0 electrons per $Å^2$ over 50 frames. The pixel size of the specimen was 0.85 Å. The data were acquired using the beam-image shift method for 3 × 3 holes with a targeted stage shift to the central hole using the SerialEM software (Schorb et al., 2019). The defocus range was set from −0.6 to −1.8 μm with 0.15 μm increments.

Cryo-EM data processing was performed using RELION 3.0.8− and 3.1− (Zivanov et al., 2018). Raw movie stacks were motion-corrected using motion correction implemented in RELION. The Contrast transfer function (CTF) parameters were determined using the CTFFIND4 program (Rohou and Grigorieff, 2015). The data processing workflow is summarized in Figure S2. A small dataset consisting of 1,467 movies from the screening session was used to obtain the initial model, and a monomeric mask for 3D classification and refinement was used to obtain a 3.9 Å map as a consensus map after CtfRefine and Basian polishing using 456,991 particles for the large dataset consisting of 5,743 movies. The large dataset contains many particles close to each, similar to that in a dimer, as shown in the result of the reference-free 2D classification in Figure S2, possibly due to concentration after purification via gel filtration. Further classification without alignment and tau_fudge2 value of 30 in two classes resulted in a better-looking model with 55.7% particles. For 254,883 particles, refinement with sidesplitter was performed to obtain a map with global resolution of 3.4 Å. Then, the focused classification without alignment and tau_fudge2 value of 20 was performed for the region around the expected EP4-Gs interface site. The particle set consisting of 178,217 particles was selected for one of the four classes, and the subtracted signal was reverted for further refinement. The selected signal-reverted particle set was used for the 3D reconstruction using refined parameters from the previous 3D refinement job to obtain two half maps for the post-process job. The particle set was further processed with CtfRefine, Basian polishing, and another CtfRefine before the 3D refinement to obtain the final map. All the resolutions reported in this article were estimated using gold-standard Fourier shell correlation (FSC) between the two independently refined half maps (FSC = 0.143). The cryo-EM maps have been deposited in the Electron Microscopy Data Bank. The statistics of EM data processing and refinement parameters are summarized in Table 1. Structural representations were generated using Chimera (Pettersen et al., 2004) and ChimeraX (Goddard et al., 2018).

Model Building and Refinement

The initial model was built from the crystal structure of the EP4-Fab001 complex (PDBID: 5YWY) (Toyoda et al., 2019) for EP4 and from the cryo-EM structure of the A_{2A}-Gs$\beta_1\gamma_2$-Nb35 complex for Gs$\beta_1\gamma_2$ and Nb35 (García-Nafría et al., 2018). The model was fitted to the EM density map using UCSF Chimera (Pettersen et al., 2004). Then, the model was further manually fitted using COOT (Emsley and Cowtan, 2004) and refined using phenix.real_space_refine (Afonine et al., 2018) within the PHENIX (Adams et al., 2010). The hydrogen atoms were added to the model during the refinement to keep the geometry of the side chains. The side chains of the residues corresponding to the poor density of the map were removed. The model geometry was validated using MolProbity (Davis et al., 2007) within the PHENIX. The final model statistics are shown in Table 1. The 3D models were deposited in the RCSB Protein Data Bank. Structural representations were generated using Pymol (Schrödinger), Chimera (Pettersen et al., 2004), and ChimeraX (Goddard et al., 2018).

GloSensor cAMP Assay

Human EP4 was inserted into pcDNA3.1 (Thermo Fisher Scientific) for expressing in HEK293 cells. The deletion sites and N-linked glycosylation site mutations were the same as in the Sf9 expression construct. The hemagglutinin and FLAG tag sequences were added at the N-terminus. This plasmid is referred to as pcDNA3.1-EP4 in this study. The site-directed mutations were introduced using polymerase chain reaction (PCR) using the designed primers.

HEK293 cells (0.5×10^6 / well) were cultured in 6-well tissue culture plates (Techno Plastic Products) at 37°C in the presence of 5% CO_2. After 24 h, 50 ng EP4 or EP4 mutant plasmid was transfected with 1.5 μg pGloSensor-22F cAMP plasmid (Promega) using polyethyleneimine. After an additional 24 h, the cells were collected and resuspended in 1 × Hank's balanced salt solution (HBSS) (Gibco) with 1 mM D-luciferin and 5 mM HEPES (pH 7.5). Cells (0.5×10^4 cells were transferred to each well of the 96 well microplate (Greiner

Please cite this article in press as: Nojima et al., Cryo-EM Structure of the Prostaglandin E Receptor EP4 Coupled to G Protein, Structure (2020), https://doi.org/10.1016/j.str.2020.11.007

Bio-one). The cells were incubated for 2 h at room temperature in the dark. PGE_2 (1 pM–1 μM) and 1 μM PF-04418948 (EP2 antagonist for inhibition of endogenous EP2 activities) were added, and luminescence was measured.

QUANTIFICATION AND STATISTICAL ANALYSIS

All cryo-EM data sets were processed using RELION 3.0.8 and 3.1. and were analyzed using the software listed in the Key Resources Table. The statistical information generated from data processing, refinement, and validation are shown in Table 1.

Sigmoid curves and EC50 values, described as mean ± SEM (Figure 3C, 4B, and Table S1), were determined using Prism8. The experiments were performed in triplicates.

No other statistical analyses were performed.

Structure, Volume *29*

Supplemental Information

Cryo-EM Structure of the Prostaglandin E Receptor EP4 Coupled to G Protein

Shingo Nojima, Yoko Fujita, Kanako Terakado Kimura, Norimichi Nomura, Ryoji Suno, Kazushi Morimoto, Masaki Yamamoto, Takeshi Noda, So Iwata, Hideki Shigematsu, and Takuya Kobayashi

SUPPLEMENTARY INFORMATION

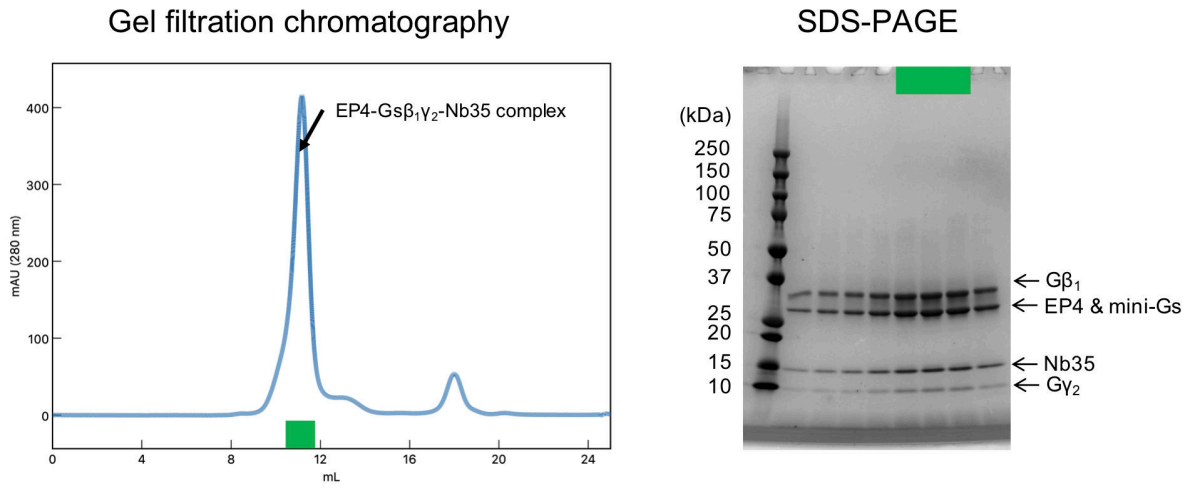

Figure S1. Purification of the PGE_2-EP4-Gs$\beta_1\gamma_2$-Nb35 complex, Related to Figure 1. Gel filtration chromatogram and SDS-PAGE of the purified PGE_2-EP4-Gs$\beta_1\gamma_2$-Nb35 complex. Green area indicates the collected fractions.

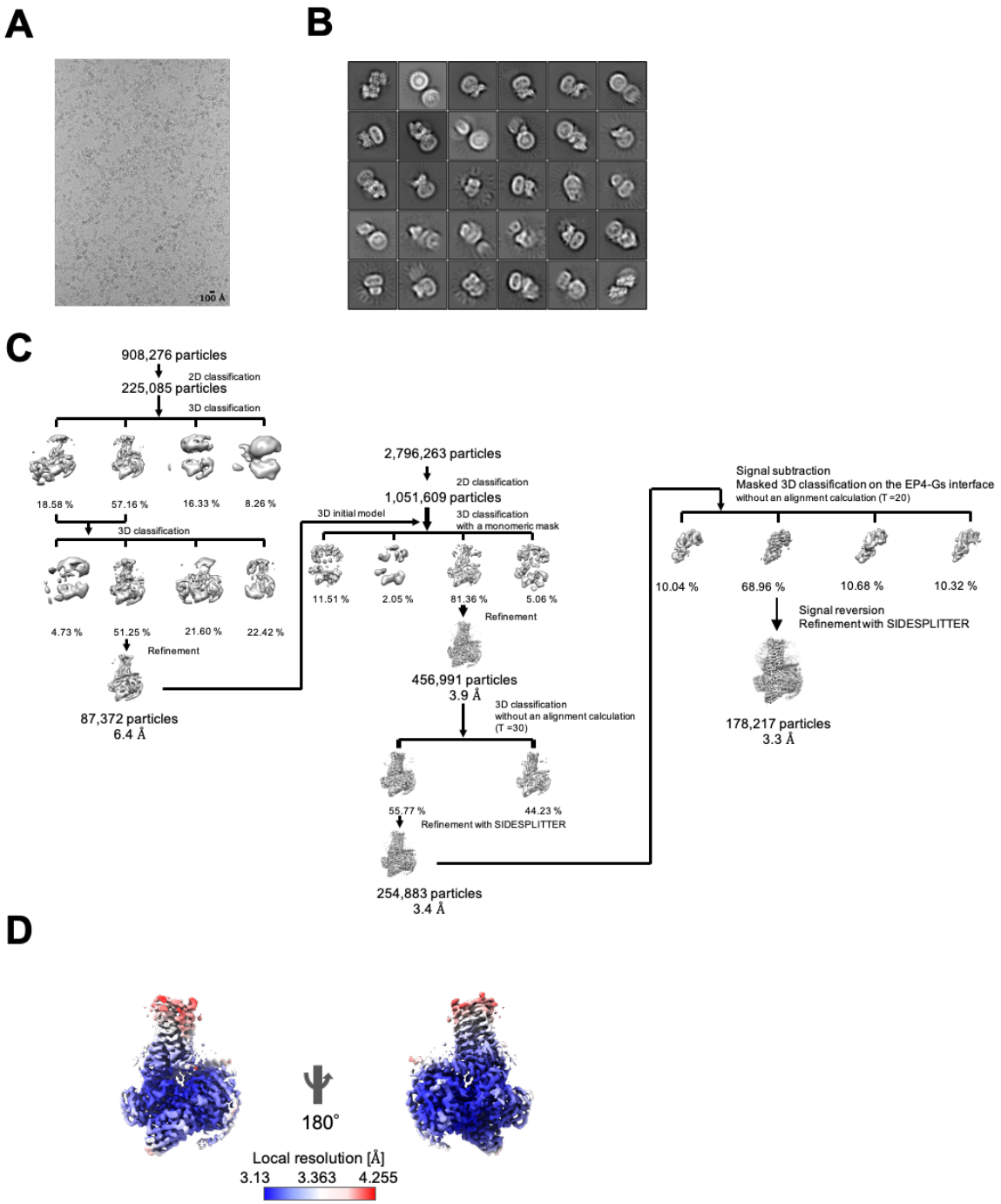

Figure S2. Cryo-EM images and single particle analysis of the PGE_2-EP4-$Gs\beta_1\gamma_2$-Nb35 complex, Related to Figure 1 and STAR Methods. (A) Representative cryo-EM micrograph of PGE_2-EP4-$Gs\beta_1\gamma_2$-Nb35 complex. (B) 2D class averages of the complex. (C) Particle classification and refinement. (D) Local resolution map of the PGE_2-EP4-$Gs\beta_1\gamma_2$-Nb35 complex.

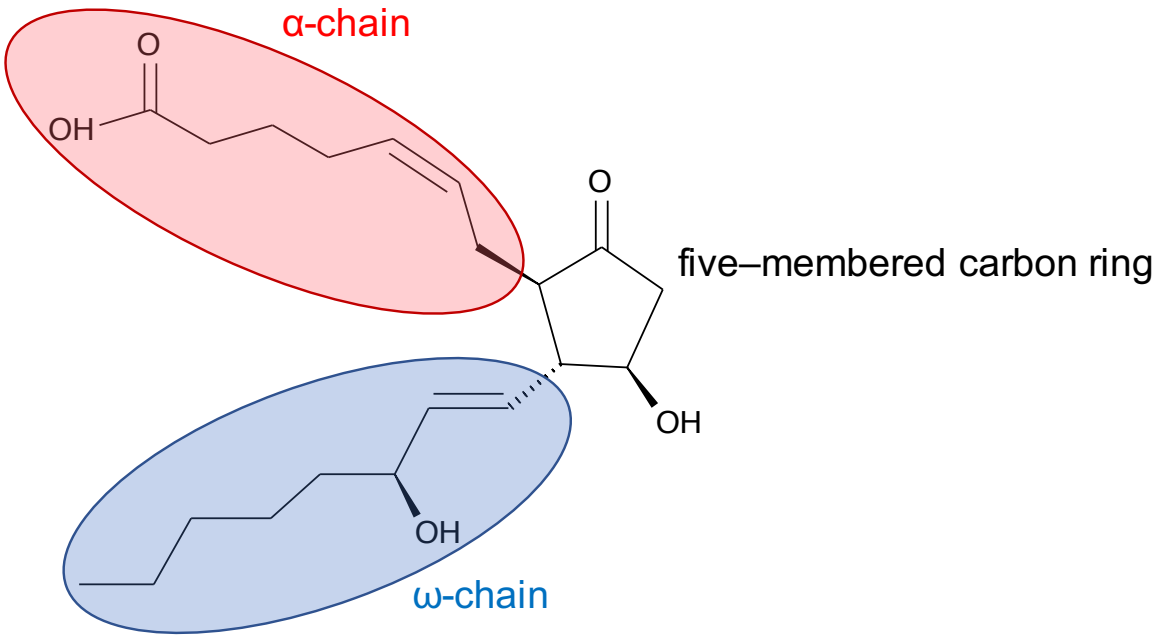

Figure S3. The structural formula of PGE_2, Related to Figure 1 and 3. The chain circled by the red ring indicates α-chain, and the chain circled by the blue ring indicates ω-chain.

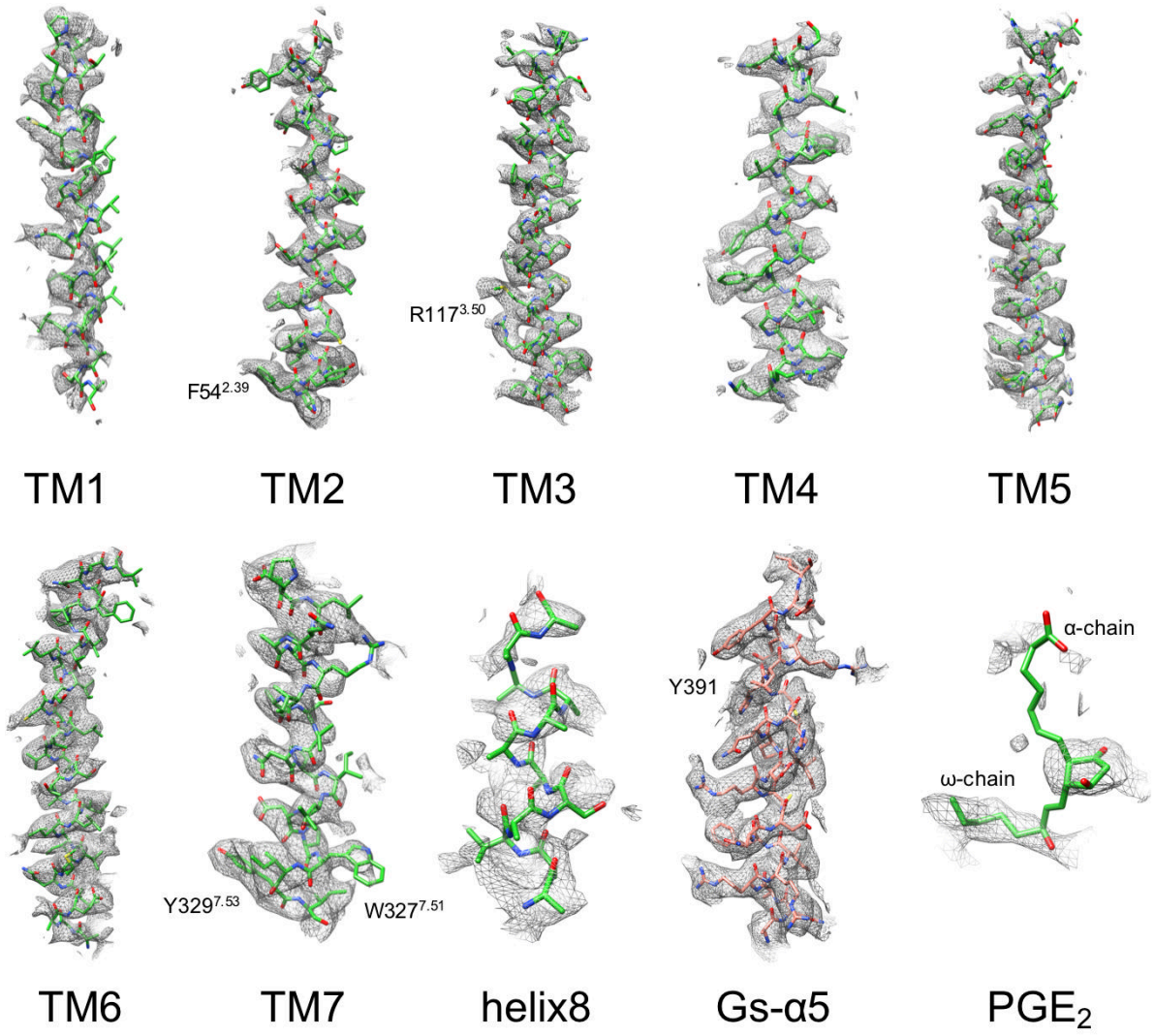

Figure S4. EM density of EP4, Gs, and PGE_2, Related to Figure 1. The EM density map at global resolution of 3.3 Å and models are shown for TM1–TM7 and helix8 of EP4, α5 of Gs, and PGE_2. The contour level of the map is set to 0.022.

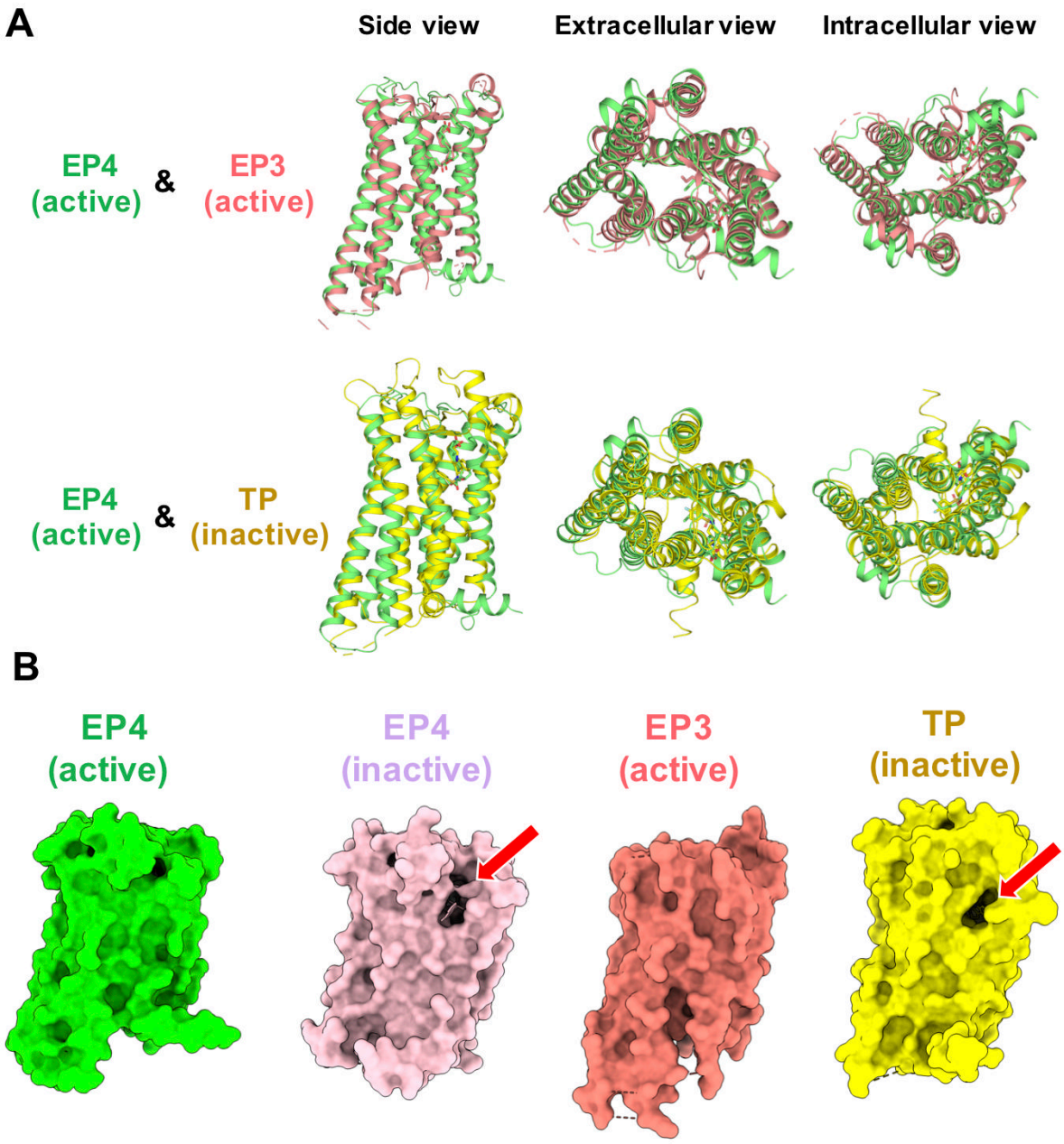

Figure S5. Structural comparison among prostanoid receptors, Related to Figure 3. (A) Comparison of the structures of active EP4 and active EP3 (PDB ID: 6AK3), and active EP4 and inactive TP (PDBID: 6IIU). Green: EP4, salmon: EP3, and yellow: TP. (B) The surface of active EP4, inactive EP4, EP3, and TP. Red arrows indicate the gap structure.

Table S1. LogEC50s obtained in signaling analysis of EP4 site-directed mutants, Related to Figure 3 and 4.

	LogEC50 Mean ± SEM
No mutation	–9.006 ± 0.04048
P24A	–7.069 ± 0.02823
M27A	–6.818 ± 0.04317
K50A	–7.798 ± 0.02671
F54A	ND
T69A	–8.138 ± 0.01655
S73G	–8.084 ± 0.02732
T76A	–7.375 ± 0.04862
Y80A	–6.721 ± 0.0411
L99A	–7.565 ± 0.04234
S103A	–8.239 ± 0.05787
E116A	–6.305 ± 0.9801
R117A	ND
Y125A	–7.348 ± 0.01942
T168A	–6.469 ± 0.3968
W169A	ND
F171A	ND
L288A	–7.685 ± 0.05319
L312A	–6.942 ± 0.04485
I315A	–7.74 ± 0.04582
R316A	ND
N321A	–6.721 ± 0.0411
R333A	–7.711 ± 0.04534